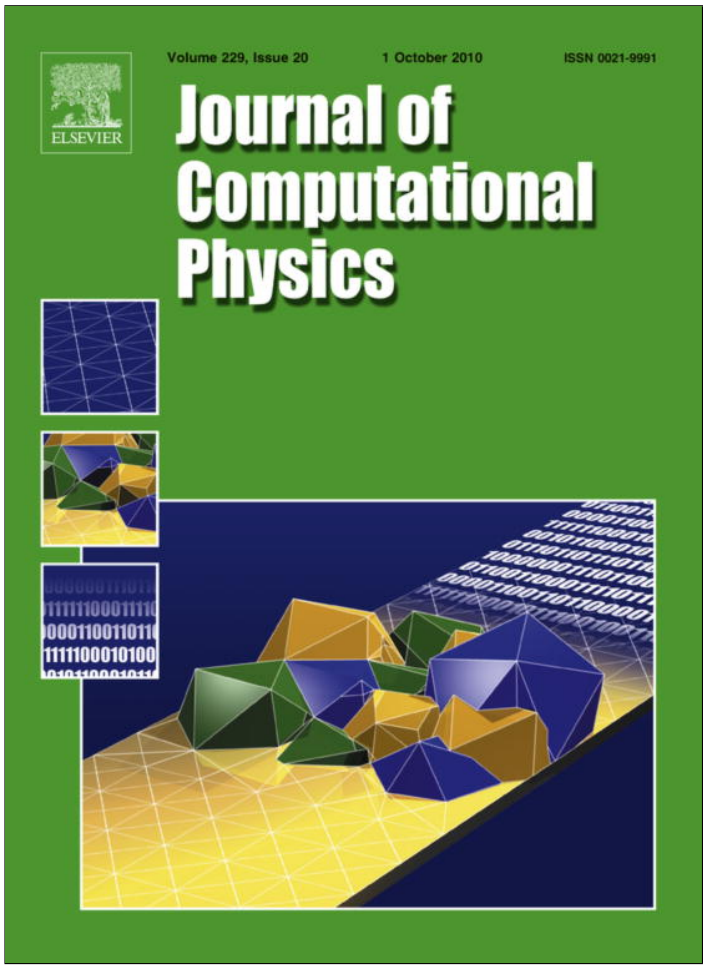

Journal of Computational Physics 229 (2010) 7956–7976

Contents lists available at ScienceDirect

Journal of Computational Physics

journal homepage: www.elsevier.com/locate/jcp

# A lattice Boltzmann model for coupled diffusion

Christian Huber [a,d,*], Bastien Chopard [b], Michael Manga [c]

[a] Department of Earth and Planetary Science, University of California – Berkeley, 307 McCone Hall 4767, Berkeley, CA 94720-4767, USA
[b] Computer Science Department, University of Geneva, CUI, 7 route de Drize, 1227 Carouge, Switzerland
[c] Department of Earth and Planetary Science, University of California – Berkeley, 177 McCone Hall 4767, Berkeley, CA 94720-4767, USA
[d] School of Earth and Atmospheric Sciences, Georgia Institute of Technology, 311 Ferst Drive, Atlanta, GA 30332, USA

ARTICLE INFO

*Article history:*
Received 11 August 2008
Received in revised form 10 June 2010
Accepted 1 July 2010

*Keywords:*
Lattice Boltzmann
Diffusion
Multicomponent
Coupling
Advection
Convection

ABSTRACT

Diffusion coupling between different chemical components can have significant effects on the distribution of chemical species and can affect the physico-chemical properties of their supporting medium. The coupling can arise from local electric charge conservation for ions or from bound components forming compounds. We present a new lattice Boltzmann model to account for the diffusive coupling between different chemical species. In this model each coupling is added as an extra relaxation term in the collision operator. The model is tested on a simple diffusion problem with two coupled components and is in excellent agreement with the results obtained through a finite difference method. Our model is observed to be numerically very stable and unconditional stability is shown for a class of diffusion matrices. We further develop the model to account for advection and show an example of application to flow in porous media in two dimensions and an example of convection due to salinity differences. We show that our model with advection loses the unconditional stability, but offers a straight-forward approach to complicated two-dimensional advection and coupled diffusion problems.



## 1. Introduction

Diffusion processes play a major role in the transport of heat and chemical components in nature. They have been shown to play an important role in the mass balance and element distribution in lakes and oceans [24,31] as well as the composition of minerals at the crystal scale. When multiple chemical components diffuse simultaneously, coupling of each component can arise because of local charge conservation for the case of ions or because the different components interact through bonds to form larger diffusing compounds. Physical and numerical models for multicomponent diffusion must account for these coupling effects. The multicomponent diffusion problem is usually described by a diffusion matrix where the non-diagonal terms represent the coupling interaction between the different diffusing species. The determination of the non-diagonal terms of the diffusion matrix is difficult as it depends on the collective behavior of all diffusing species present. The general approach used to determine these coefficients is semi-empirical, where the theoretical basis is described by Onsager's theory for non-equilibrium thermodynamics [28,29,25–27]. The non-diagonal terms of the diffusion matrix can be related to Onsager's phenomenological coefficients, however explicit relationships require experimental measurements [26,16,17,8,9].

Various multicomponent transport models have been developed for a macroscopic description of the transport equations using finite differences [8], finite volume and finite element methods [23]. However, these methods prove to be challenging

* Corresponding author at: School of Earth and Atmospheric Sciences, Georgia Institute of Technology, 311 Ferst Drive, Atlanta, GA 30332, USA.
*E-mail addresses:* chuber@seismo.berkeley.edu, christian.huber@eas.gatech.edu (C. Huber), Bastien.Chopard@unige.ch (B. Chopard), manga@seismo.berkeley.edu (M. Manga).

0021-9991/$ - see front matter © 2010 Elsevier Inc. All rights reserved.
doi:10.1016/j.jcp.2010.07.002

when dealing with transport in complex geometries (porous media). Over the last two decades, the lattice Boltzmann (LB) method has emerged as a powerful alternative to standard computational methods. The lattice Boltzmann method is an extension of lattice gas automata [10] based on a mesoscale statistical description where the dynamics is reduced to the propagation and collision of pseudo-particles [10,18,30]. Distributions of pseudo-particles relax to a local equilibrium defined by the local macroscopic fields (concentration, density, velocity) through a collision operator and can be applied to a wide range of applications such as for instance complex fluid dynamics, reaction–diffusion processes or wave propagation [2,34]. The collision operator is generally simplified as a simple relaxation to a prescribed local equilibrium function depending on the conserved quantities. Single relaxation time models are commonly referred to as BGK dynamics [1,30]. Multi-relaxation time models (MRT) have been developed to address some issues encountered with single relaxation BGK models. For example, they offer additional free parameters that can be tuned to offer better stability, more accurate boundary conditions and reduce numerical diffusion for advection–diffusion models [6,7,11–13]. Due to their statistical nature, lattice Boltzmann methods offer the advantage of using simple local rules for liquid–solid boundaries (bounce-back of the local particle distribution functions) and are often very easily and efficiently parallelized. In addition LB models directly give the value of the shear stress (hydrodynamics) or particle flux (diffusion processes) without the need to compute finite-differences.

In this study, we develop a new lattice Boltzmann approach for multicomponent diffusion based on a modification of the standard BGK collision operator for one species. Although we do not present a version of our model with a multiple-relaxation time collision operator, our model can be generalized in a straight-forward way. In the next section, we introduce the equation for multicomponent diffusion. We then present the modified BGK diffusion model to include the effect of coupling between components. We show through a Chapman–Enskog expansion that the model converges to the correct set of macroscopic equations. We then present an analysis of the stability and accuracy of the model. We modify the model further to include the effects of advection of the supporting media (e.g. aqueous solution). The model for multicomponent diffusion in the absence of flow is compared to the solutions obtained with a finite difference model. Finally, we present an application for the advection-multicomponent diffusion in porous media that requires no subsequent modification of the presented scheme to illustrate the versatility and simplicity of the method.

## 2. Multicomponent coupled diffusion

Multicomponent coupled diffusion is usually described in terms of a diffusion matrix representing the couplings between the different chemical species. In one dimension, it is usually written as

$$\frac{\partial C_j}{\partial t} = \sum_k \frac{\partial}{\partial x}\left[D_{jk}\frac{\partial C_k}{\partial x}\right], \tag{1}$$

where the diagonal components of the matrix $D_{jk}$ represent the self-diffusion coefficients and the non-diagonal terms represent the coupling between element $j$ and $k$. Onsager's theory predicts that the diffusion matrix has to be symmetric, however, owing to other constraints such as charge conservation, the diffusion matrix is usually not symmetric. We develop and validate a new lattice Boltzmann model to incorporate the diffusion coupling between different chemical components under the assumption that the elements of the diffusion matrix $D_{jk}$ are constants, i.e. $D_{jk} \neq D_{jk}(C_j, C_k)$. This limitation can easily be avoided by adjusting the relaxation times of the BGK dynamics locally and/or at every time step [15].

## 3. Lattice Boltzmann scheme for coupled diffusion

The model we introduce here is based on the standard BGK collision scheme for diffusion [38,3], where the concentration of species $C_n$ is described by the an evolution equation for particle distribution functions $f_i^n$

$$f_i^n(\mathbf{x} + \delta_t \mathbf{e}_i, t + \delta_t) = (1 - \omega_n) f_i^n(\mathbf{x}, t) + \omega_n f_i^{n0}(\mathbf{x}, t), \tag{2}$$

where the superscripts $n = 1, \ldots, p$ refer to the species and index $i$ labels the lattice velocities $\mathbf{e}_i$. These velocity vectors are such that in one time step $\delta_t$, the particles can hop from their initial position $\mathbf{x}$ to $\mathbf{x} + \delta_t \mathbf{e}_i$, still on the lattice.

Different lattices can be considered in the LB method. They are termed D$d$Q$q$, where $d$ is the space dimension and $q$ the number of velocity vectors. For instance the so-called D2Q5 lattice corresponds to a two-dimensional square lattice with five velocities (rest, east, north, west and south).

For symmetry and isotropy reasons, the $\mathbf{e}_i$ must obey

$$\sum_i t_i \mathbf{e}_i = 0, \quad \sum_i t_i \mathbf{e}_{i\alpha}\mathbf{e}_{i\beta} = e_s^2 \delta_{\alpha\beta}, \quad \sum_i t_i = 1, \tag{3}$$

where greek indices $\alpha$ and $\beta$ denote the spatial components of $\mathbf{e}_i$. The $t_i$'s and $e_s^2$ are positive constants which depend on the chosen lattice. For instance, here we chose $t_0 = 1/3$, $t_{i\neq 0} = 1/6$ and $e_s^2 = 1/3$ in the D2Q5 lattice.

In a LB approach, the standard physical quantities are given by the moments of the distribution functions $f_i$. In diffusion problems the density $C_n$ is computed as

$$C_n = \sum_i f_i^n. \tag{4}$$

In Eq. (2), $f_i^{n0}$ are the so-called local equilibrium distribution functions defined as

$$f_i^{n0} = t_i C_n.$$

The $\omega_n$'s are the inverse of the relaxation time for species $n$ and can be chosen [38,3] so as to impose the desired diffusion constant, according to the relation $D_n = e_s^2 \delta_t (1/\omega_n - 1/2)$. An interesting result is that, in the absence of an advecting velocity field, the diffusive flux $\mathbf{J}_n$ is found to satisfy

$$\mathbf{J}_n = \left(1 - \frac{\omega_n}{2}\right) \sum_i (f_i^n - f_i^{n0}) \mathbf{e}_i = -D_n \nabla C_n. \tag{5}$$

The goal of this paper is to generalize Eq. (2) to the case of coupled diffusion among several species. The equation for $\mathbf{J}$ and relation (1) suggest an approach to couple species by adding to Eq. (2) terms involving contributions from $(f_i^k - f_i^{k0})$, i.e. terms containing the gradient of density $C_k$. Thus, we introduce non-diagonal terms in the diffusion matrix as

$$f_i^n(\mathbf{x} + \delta_t \mathbf{e}_\mathbf{i}, t + \delta_t) = (1 - \omega_n) f_i^n(\mathbf{x}, t) + \omega_n f_i^{n0}(\mathbf{x}, t) - \sum_{k \neq n} \omega_{nk} \left(f_i^{k0}(\mathbf{x}, t) - f_i^k(\mathbf{x}, t)\right). \tag{6}$$

To simplify the notation, we omit position and time when possible and we focus on the one-way coupling of species $C_1$ with species $C_2$ described, respectively by the particle distributions $f_i$ and $g_i$. The evolution of these distributions is given by

$$f_i(\mathbf{x} + \delta_t \mathbf{e}_\mathbf{i}, t + \delta_t) = (1 - \omega_f) f_i(\mathbf{x}, t) + \omega_f f_i^0(\mathbf{x}, t) - \omega_{fg} \left(g_i^0(\mathbf{x}, t) - g_i(\mathbf{x}, t)\right) \tag{7}$$

and

$$g_i(\mathbf{x} + \delta_t \mathbf{e}_\mathbf{i}, t + \delta_t) = (1 - \omega_g) g_i(\mathbf{x}, t) + \omega_g g_i^0(\mathbf{x}, t) - \omega_{gf} \left(f_i^0(\mathbf{x}, t) - f_i(\mathbf{x}, t)\right). \tag{8}$$

The equilibrium distributions are given, as before, by

$$f_i^0 = t_i C_1 \quad \text{and} \quad g_i^0 = t_i C_2. \tag{9}$$

We now show that, in the continuous limit (mesh size and time step going to zero), the two systems of Eqs. (7) and (8) are equivalent to Eq. (1). We use the multiscale Chapman–Enskog expansion (see for instance Frisch et al. [10], Chopard and Droz [2] for more details).

Assuming that the $f_i$ are smooth functions, and that time and space scale diffusively ($x^2 \sim t$), a second order Taylor expansion in $\delta_t$ yields

$$f_i(\mathbf{x} + \delta_t \mathbf{e}_i, t + \delta_t) = f_i(\mathbf{x}, t) + \delta_t \partial_\alpha e_{i\alpha} f_i(\mathbf{x}, t) + \delta_t \partial_t f_i(\mathbf{x}, t) + \frac{\delta_t^2}{2} e_{i\alpha} e_{i\beta} \partial_\alpha \partial_\beta f_i(\mathbf{x}, t) \tag{10}$$

and similarly for $g_i$. Here, $\partial_\alpha$ denotes the derivative with respect to spatial coordinate $\alpha$ and $\partial_t$ is the time derivative. We use the summation convention over repeated greek indices.

The next step is to expand $f_i$ and $g_i$ in terms of the local equilibrium distribution. For the case of $f_i$, we write

$$f_i = f_i^0 + \epsilon f_i^{(1)}, \tag{11}$$

where $f_i^{(1)}$ is defined as the non-equilibrium part of the distribution and $\epsilon$ is an expansion parameter (related to the Knudsen number).

We expand the partial derivatives as

$$\partial_t = \epsilon^2 \partial_t^{(2)}, \quad \partial_\alpha = \epsilon \partial_\alpha^{(1)}. \tag{12}$$

Equating Eqs. (7) and (10) and doing the same for the distributions $g_i$, we obtain, at order $\mathcal{O}(\epsilon)$, the following conditions for the non-equilibrium part of the distribution $f_i^{(1)}$ and $g_i^{(1)}$

$$\begin{aligned} \epsilon f_i^{(1)} &= \epsilon \frac{\omega_{fg}}{\omega_f} g_i^{(1)} - \epsilon \frac{\delta_t}{\omega_f} \partial_\alpha^{(1)} e_{i\alpha} f_i^0, \\ \epsilon g_i^{(1)} &= \epsilon \frac{\omega_{gf}}{\omega_g} f_i^{(1)} - \epsilon \frac{\delta_t}{\omega_g} \partial_\alpha^{(1)} e_{i\alpha} g_i^0. \end{aligned} \tag{13}$$

From Eq. (7), the definition of the equilibrium distribution

$$\sum_i f_i = \sum_i f_i^0 = C_1, \quad \sum_i g_i = \sum_i g_i^0 = C_2 \tag{14}$$

and using Eq. (10), we have (up to second order in $\epsilon$)

$$0 = \sum_i [f_i(\mathbf{x}+\mathbf{e_i}, t+1) - f_i(\mathbf{x}, t)] = \epsilon \sum_i e_{i\alpha}\partial_\alpha^{(1)} f_i^{(0)} + \epsilon^2 \sum_i \left[\partial_\alpha^{(1)} e_{i\alpha} f_i^{(1)} + \partial_t^{(2)} f_i^0 + \frac{\delta_t}{2}\partial_\alpha^{(1)}\partial_\beta^{(1)} e_{i\alpha} e_{i\beta} f_i^0\right]. \tag{15}$$

By the symmetry of the $\mathbf{e}_i$'s and the definition of $f_i^{(0)}$, we have $\sum_i e_{i\alpha}\partial_\alpha^{(1)} f_i^{(0)} = 0$. Therefore, with $\mathbf{C} = (C_1, C_2)$, the symmetries of the lattice equations (3) and (12), we obtain

$$\partial_t \mathbf{C} = -\epsilon^2 \sum_i \left[\partial_\alpha^{(1)} e_{i\alpha} f_i^{(1)}\right] - \delta_t \frac{e_s^2}{2}\nabla^2 \mathbf{C}. \tag{16}$$

We now define

$$\begin{aligned} &\mathbf{X}_i^0 = \begin{pmatrix} f_i^0 \\ g_i^0 \end{pmatrix}, \quad \mathbf{X}_i^{(1)} = \begin{pmatrix} f_i^{(1)} \\ g_i^{(1)} \end{pmatrix}, \\ &\mathbf{M} = \begin{pmatrix} 1 & -\frac{\omega_{fg}}{\omega_f} \\ -\frac{\omega_{gf}}{\omega_g} & 1 \end{pmatrix}, \quad \mathbf{K} = \begin{pmatrix} -\frac{1}{\omega_f} & 0 \\ 0 & -\frac{1}{\omega_g} \end{pmatrix}. \end{aligned} \tag{17}$$

Eq. (13) then read

$$M\mathbf{X}_i^{(1)} = \delta_t K \partial_\alpha^{(1)} e_{i\alpha}\mathbf{X}_i^{(0)} \quad \text{or} \quad \mathbf{X}_i^{(1)} = \delta_t M^{-1} K \partial_\alpha^{(1)} e_{i\alpha}\mathbf{X}_i^{(0)}, \tag{18}$$

provided that $\omega_f\omega_g - \omega_{fg}\omega_{gf} \neq 0$. The first term of the right-hand side of Eq. (16) can thus be calculated as

$$\epsilon^2 \sum_i \partial_\alpha^{(1)} e_{i\alpha}\mathbf{X}_i^{(1)} = \delta_t \mathbf{M}^{-1}\mathbf{K} \sum_i \epsilon^2 \partial_\alpha^{(1)}\partial_\beta^{(1)} e_{i\alpha} e_{i\beta}\mathbf{X}_i^0, \tag{19}$$

$$= e_s^2 \delta_t \mathbf{M}^{-1}\mathbf{K}\nabla^2\mathbf{C}. \tag{20}$$

Eq. (16) becomes

$$\partial_t \mathbf{C} = -e_s^2\delta_t\left(\mathbf{M}^{-1}\mathbf{K} + \frac{1}{2}\mathbf{I}\right)\nabla^2\mathbf{C} \equiv \mathbf{D}\nabla^2\mathbf{C}, \tag{21}$$

where $\mathbf{I}$ is the identity matrix and $\mathbf{D}$ the diffusion matrix is

$$\mathbf{D} = e_s^2\delta_t\left[\begin{pmatrix} 1 & -\frac{\omega_{fg}}{\omega_f} \\ -\frac{\omega_{gf}}{\omega_g} & 1 \end{pmatrix}^{-1}\begin{pmatrix} \frac{1}{\omega_f} & 0 \\ 0 & \frac{1}{\omega_g} \end{pmatrix} - \begin{pmatrix} \frac{1}{2} & 0 \\ 0 & \frac{1}{2} \end{pmatrix}\right]. \tag{22}$$

For a single component, the diffusion matrix reduces to its usual LB scalar expression

$$D = e_s^2\delta_t\left(\frac{1}{\omega_f} - \frac{1}{2}\right). \tag{23}$$

The two-component model above can be easily extended to $n$ components whose evolution is given by Eq. (6) provided the determinant of $\mathbf{M}$ is not null. In this case the diffusion matrix is given by

$$\mathbf{D} = e_s^2\delta_t\left[\begin{pmatrix} 1 & -\frac{\omega_{12}}{\omega_1} & \dots & -\frac{\omega_{1n}}{\omega_1} \\ -\frac{\omega_{21}}{\omega_2} & 1 & -\frac{\omega_{23}}{\omega_2} & \dots \\ \dots & \dots & \dots & \dots \\ -\frac{\omega_{n1}}{\omega_n} & \dots & \dots & 1 \end{pmatrix}^{-1}\begin{pmatrix} \frac{1}{\omega_1} & 0 & \dots & \dots \\ 0 & \frac{1}{\omega_2} & 0 & \dots \\ \dots & \dots & \dots & \dots \\ 0 & \dots & \dots & \frac{1}{\omega_n} \end{pmatrix} - \begin{pmatrix} \frac{1}{2} & 0 & \dots & \dots \\ 0 & \frac{1}{2} & 0 & \dots \\ \dots & \dots & \dots & \dots \\ 0 & \dots & \dots & \frac{1}{2} \end{pmatrix}\right]. \tag{24}$$

This equation can be inverted to calculate the $\omega$'s from a prescribed diffusion matrix. From Eq. (21)

$$-\mathbf{K}^{-1}\mathbf{M} = \left(\frac{1}{\delta_t e_s^2}D + \frac{1}{2}\mathbf{I}\right)^{-1} \tag{25}$$

and from the definitions of $\mathbf{M}$ and $\mathbf{K}$ we get

$$\left[-\mathbf{K}^{-1}\mathbf{M}\right]_{ij} = \begin{cases} \omega_i, & \text{if } i = j, \\ -\omega_{ij}, & \text{otherwise.} \end{cases} \tag{26}$$

If none of the diffusion matrix $\mathcal{D}$ eigenvalues are $-(\delta_t e_s^2/2)$, the matrix $D/(\delta_t e_s^2) + 1/2$ can be inverted and Eqs. (25) and (26) provide a direct relationship between the $\omega_i$, $\omega_{ij}$ and the diffusion matrix.

### 3.1. Semi-analytical investigation of the stability and accuracy of the single and multicomponent methods

In Appendix A, we prove analytically the unconditional stability of the lattice Boltzmann single component diffusion model. This development has not yet been generalized to the multicomponent case. Therefore, here we investigate the stability and accuracy of the LBGK for multiple components using a semi-analytical approach similar to that presented in Chopard and Droz [2] and Ginzburg [11].

To introduce our approach we first explain it in the case of the single component case. The evolution equation (2) is written as an algebraic system of linear equations

$$\mathbf{f}^{out} = \mathbf{L}\mathbf{f}^{in}, \tag{27}$$

where for a single component, using a D2Q5 lattice,

$$\mathbf{f}^{out} = \begin{pmatrix} f_0^{out} \\ \vdots \\ f_4^{out} \end{pmatrix}, \quad \mathbf{f}^{in} = \begin{pmatrix} f_0^{in} \\ \vdots \\ f_4^{in} \end{pmatrix}, \quad L_{ij} = \begin{cases} 1 - \frac{1}{\tau} + \frac{t_i}{\tau}, & \text{if } i = j, \\ \frac{t_i}{\tau}, & \text{otherwise.} \end{cases} \tag{28}$$

The distributions $\mathbf{f}$ can be written in terms of Fourier series

$$\mathbf{f}^{in}(\mathbf{x}, t) = \sum_{\mathbf{k}} \mathbf{A}_{\mathbf{k}}(t) \exp(i\mathbf{k} \cdot \mathbf{x}), \tag{29}$$

where the vectors $\mathbf{A}_{\mathbf{k}}$ have the same number of elements as the distribution vectors $\mathbf{f}$ for each wave vector $\mathbf{k}$. On a two-dimensional lattice, the wave vectors are defined by

$$\mathbf{k} = (2\pi l/(N\delta x), 2\pi m/(N\delta x)), \quad l, m = 0, 1, \ldots, N-1, \tag{30}$$

where $N$ is the number of grid nodes in each dimension and $\delta x$ the grid spacing. With this notation, Eq. (2) becomes

$$\sum_{\mathbf{k}} \mathbf{T}_{\mathbf{k}} \mathbf{A}_{\mathbf{k}}(t + \delta t) \exp(i\mathbf{k} \cdot \mathbf{x}) = \mathbf{L} \sum_{\mathbf{k}} \mathbf{A}_{\mathbf{k}}(t) \exp(i\mathbf{k} \cdot \mathbf{x}), \tag{31}$$

where $T_{\mathbf{k}}$ is a diagonal $q \times q$ matrix whose elements are

$$[T_{\mathbf{k}}]_{mn} = \begin{cases} \exp(i\mathbf{k} \cdot \mathbf{e}_m), & \text{if } m = n, \\ 0, & \text{otherwise.} \end{cases} \tag{32}$$

We can use the orthogonality of the basis $\exp(i\mathbf{k} \cdot \mathbf{x})$ to obtain

$$\mathbf{A}_{\mathbf{k}}(t + \delta_t) = \mathbf{T}_{\mathbf{k}}^{-1} \mathbf{L} \mathbf{A}_{\mathbf{k}}(t) \equiv \mathbf{P}_{\mathbf{k}} \mathbf{A}_{\mathbf{k}}(t). \tag{33}$$

If we write $A_{\mathbf{k}}(t) = e^{i\omega_{\mathbf{k}} t} A_{\mathbf{k}}(0)$ we see that a solution to Eq. (33) exists provided that $e^{i\omega_{\mathbf{k}}\delta_t}$ is an eigenvalue $\lambda_{\mathbf{k}}$ of $P_{\mathbf{k}}$. The relation $e^{i\omega_{\mathbf{k}}\delta_t} = \lambda_k$ specifies the dispersion relation between $\omega_{\mathbf{k}}$ and the wave vector $\mathbf{k}$.

Solving numerically for the eigenvalues of $\mathbf{P}$, we can compare the dispersion relationship obtained for our scheme to the dispersion obtained analytically from the diffusion equation

$$i\omega = -k^2 D \quad \text{or} \quad e^{i\omega} = e^{-k^2 D}, \tag{34}$$

where $D$ is the diffusivity.

Fig. 1 shows the comparison between the dispersion relationship obtained from the eigenvalues of the operator $\mathbf{P}_{\mathbf{k}}$ and Eq. (34) for a single component with two different relaxation time values.

The unconditional stability of the scheme requires that $\mathbf{P}_{\mathbf{k}}$ does not admit an eigenvalue bigger than one for every choice of $\mathbf{k}$ and $\tau$. Fig. 1(a) and (c) are representative of the main features observed with this analysis. Stability does not depend on the choice of relaxation time (when $\tau > 0.5$) but the accuracy of the method depends both on the resolution (higher resolution at small $\mathbf{k}$) and the choice of $\tau$ (better for small $\tau$). Fig. 1(b) and (d) show the order of accuracy of the LBGK method for single component diffusion. The error on the dispersion equation grows as $k^4$ for any choice of $\tau$, showing that the LB method captures the second order derivatives correctly.

The multicomponent diffusion model can be analyzed in a similar way. For simplicity we investigate the case of two components described, respectively, by the evolution equations (7) and (8). We define the post and pre-collision operators $\mathbf{f}^{out}$, $\mathbf{f}^{in}$ and the matrix $\mathbf{L}$

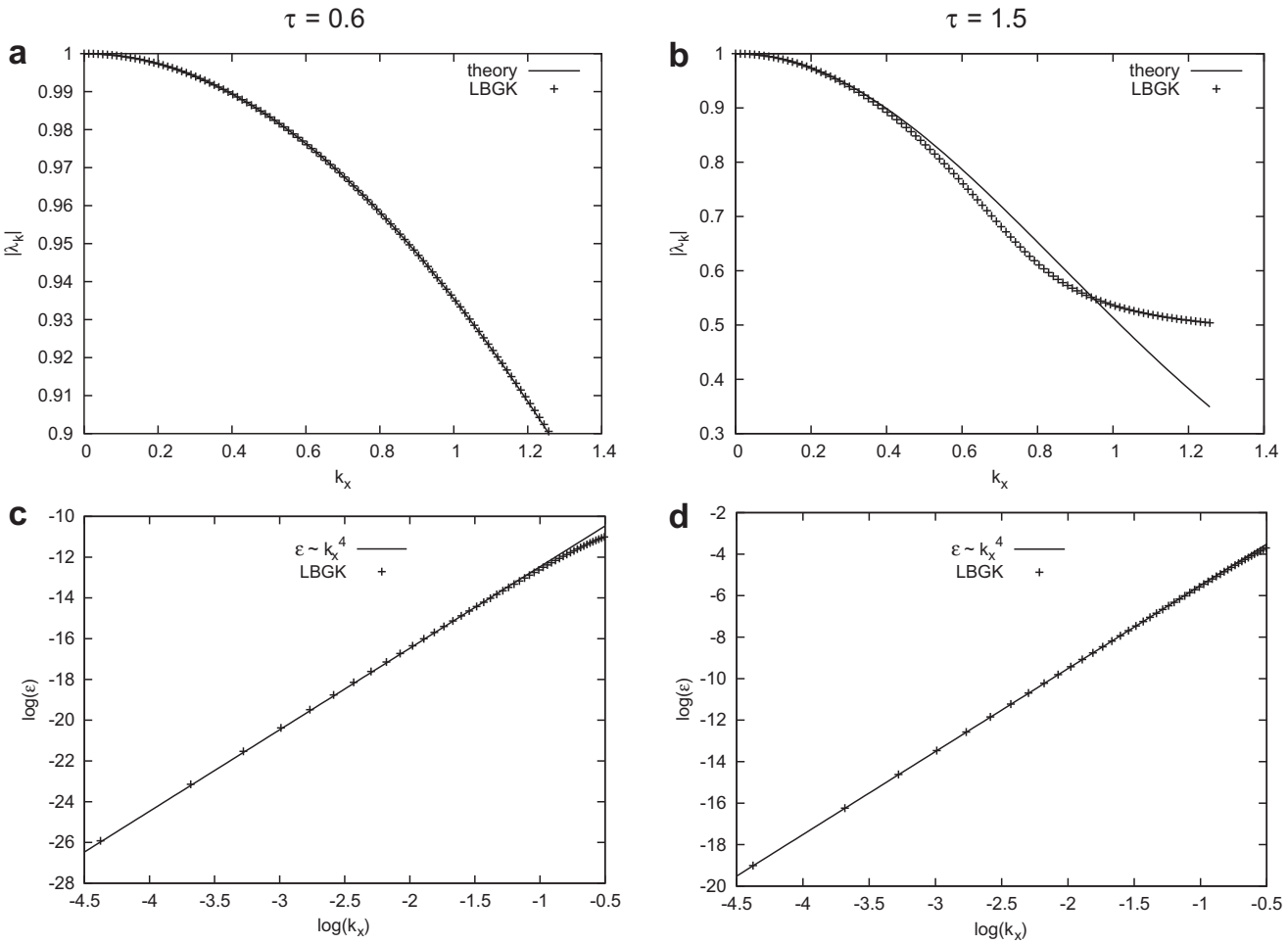


**Fig. 1.** Largest eigenvalue of the matrix **P** as function of the $x$-component of the wave vector $\mathbf{k}$ ($k_y = k_x$ here) for the diffusion of a single component. For comparison, the expected result obtained from the analytical expression of the dispersion equation is also plotted. (a) Case for $\tau = 0.6$. (c) Error, i.e. difference between the analytical result obtained from the dispersion equation and the results obtained from the numerical scheme. (b) and (d) same plots for $\tau = 1.5$.

$$\mathbf{f}^{out} = \begin{pmatrix} f_0^{out} \\ \vdots \\ f_4^{out} \\ g_0^{out} \\ \vdots \\ g_4^{out} \end{pmatrix}, \quad \mathbf{f}^{in} = \begin{pmatrix} f_0^{in} \\ \vdots \\ f_4^{in} \\ g_0^{in} \\ \vdots \\ g_4^{in} \end{pmatrix}, \quad \mathbf{L} = \begin{pmatrix} \mathbf{L}_{s,f} & \mathbf{L}^{fg} \\ \mathbf{L}^{gf} & \mathbf{L}_{s,g} \end{pmatrix}. \tag{35}$$

The evolution of the distributions becomes

$$\mathbf{f}^{out} = \mathbf{L}\mathbf{f}^{in}. \tag{36}$$

The matrix $\mathbf{L}$ is now a $2q \times 2q$ matrix (where $q$ is defined by the D2Q$q$ lattice used for the diffusion problem) and where the diagonal blocks of size $q \times q$ are similar to the matrix $\mathbf{L}$ of Eq. (28) for each distribution. The elements of the off-diagonal blocks are

$$[L^{mn}]_{ij} = \begin{cases} \frac{1}{\tau_{mn}} - \frac{t_i}{\tau_{mn}}, & \text{if } i = j, \\ -\frac{t_i}{\tau_{mn}}, & \text{otherwise,} \end{cases} \quad \text{where } m, n = f, g. \tag{37}$$

A discrete Fourier transform leads to the same algebraic equations as for the single component case

$$\mathbf{A}_{\mathbf{k}}(t + \delta t) = \mathbf{P}_{\mathbf{k}}\mathbf{A}_{\mathbf{k}}(t). \tag{38}$$

$\mathbf{P}_{\mathbf{k}}$ is defined by

$$\mathbf{P}_{\mathbf{k}} = \mathbf{T}_{\mathbf{k}}^{-1}\mathbf{L} \tag{39}$$

with $\mathbf{T}_{\mathbf{k}}$ a $2q \times 2q$ diagonal matrix repeating twice the matrix $\mathbf{T}_{\mathbf{k}}$ of Eq. (32).

Similar to the single component diffusion case, the eigenvalues of $P_{\mathbf{k}}$ give the dispersion relation of the LB model and can be used to check its ability to reproduce Eq. (1).

Calculating the Fourier transform in both space and time of Eq. (1) for two components, gives the following dispersion relationship

$$\det\left[i\omega + k^2 \underbrace{\begin{pmatrix} D_f & D_{fg} \\ D_{gf} & D_g \end{pmatrix}}_{\mathcal{D}}\right] = 0, \tag{40}$$

where $\mathcal{D}$ is the diffusion matrix. The solutions to this dispersion equation are $i\omega_\pm = -k^2\lambda_\pm$, with $\lambda_\pm$ the eigenvalues of $k^2\mathcal{D}$

$$\lambda_\pm = \frac{1}{2}\left(D_f + D_g \pm \sqrt{(D_f - D_g)^2 + 4D_{fg}D_{gf}}\right). \tag{41}$$

Note that for uncoupled diffusing species ($D_{fg} = D_{gf} = 0$) the eigenvalues become $\lambda_+ = D_f$ and $\lambda_- = D_g$, as expected. To compare this dispersion relation with our lattice Boltzmann model, we compare

$$\exp(i\omega_\pm) = \exp\left[-\frac{k^2}{2}\left(D_f + D_g \pm \sqrt{(D_f - D_g)^2 + 4D_{fg}D_{gf}}\right)\right] \tag{42}$$

with the eigenvalues of $\mathbf{P_k}$, defined in Eq. (39).

Figs. 2 and 3 show dispersion equation (42), together with the two largest eigenvalues of the evolution matrix ($\mathbf{P_k}$) of the lattice Boltzmann model. Owing to the symmetry of the eigenvalues for $k$ and $2\pi - k$, we show only the first half of the wave vector values in the left panels. In the right panels, only the first quarter of the wave vector values are shown. We observe

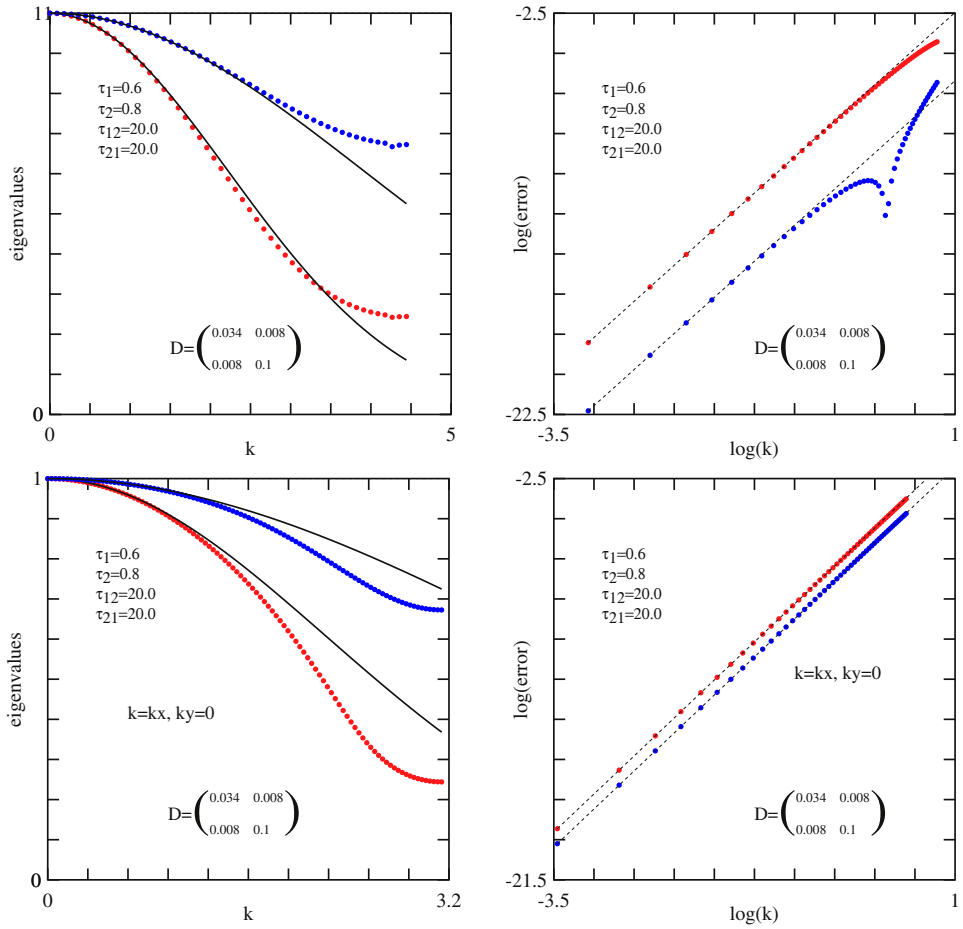


**Fig. 2.** Left: Comparison of the eigenvalues of the lattice Boltzmann model and the exponential of the dispersion relation of the coupled diffusion PDE. Right: Error between the curves on the left, on a log–log scale. The dashed line of slope 4 shows that for both eigenvalues, the error grows as $k^4$ meaning that first and second order derivatives are correctly computed in the LB model. The quantity $k$ is defined as $k = \sqrt{k_x^2 + k_y^2}$. In the upper plots, we chose $k_x = k_y$ and in the lower plots $k_y = 0$.

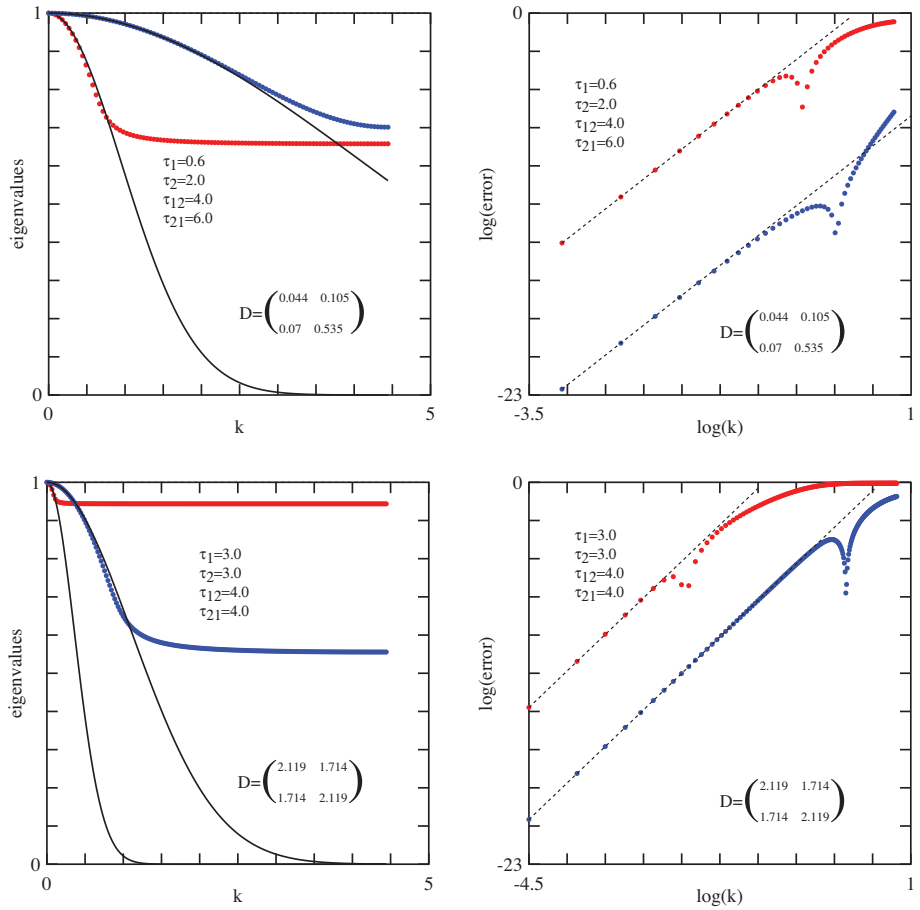


**Fig. 3.** Same as Fig. 2 but for other diffusion coefficients and for $k_x = k_y$ in all cases.

that the two eigenvalues, which represent the mass conservation in the model, agree with dispersion relation (42) with an error that grows as $k^4$. The model is therefore in agreement with the partial differential equation up to second order, consistent with our Chapman–Enskog development. As the diffusion coefficients increase, the range of $k$ values for which the error is "small" tends to decrease, therefore a larger lattice is required to avoid inaccuracy associated with small wavelengths.

The stability of the model can be investigated with a similar approach. The two-component coupled diffusion equation becomes ill-defined if the eigenvalues of $\mathcal{D}$ are negative. This necessary condition leads to the constraint

$$\left[\left(D_f + D_g \pm \sqrt{(D_f - D_g)^2 + 4D_{fg}D_{gf}}\right)\right] > 0. \tag{43}$$

The cross-diffusion coefficients must therefore be small enough compared to the diagonal terms.

In what follows we shall restrict ourselves to the case where $D_f = D_g = D$ and $D_{fg} = D_{gf}$. Then condition (43) reduces to $D > |D_{fg}|$. This constraint can be translated to the space of the relaxation frequencies. From Eqs. (25) and (26) we obtain

$$\omega_f = \omega_g = \frac{D_f/e_s^2 + 1/2}{\left(D_f/e_s^2 + 1/2\right)^2 - \left(D_{fg}/e_s^2\right)^2} \tag{44}$$

and

$$\omega_{fg} = \omega_{gf} = \frac{-D_{fg}/e_s^2}{\left(D_f/e_s^2 + 1/2\right)^2 - \left(D_{fg}/e_s^2\right)^2}. \tag{45}$$

Since $D_f$ is positive, the condition $D_f > |D_{fg}|$ ensures that the denominators of (44) and (45) are strictly positive. Therefore we have

$$\omega_f > 0, \quad \omega_f > |\omega_{fg}|. \tag{46}$$

From Eq. (25), we can also obtain the inverse relations

$$D_f = e_s^2\delta_t\left(\frac{w_f}{\omega_f^2 - \omega_{fg}^2} - \frac{1}{2}\right), \quad D_{fg} = e_s^2\delta_t\left(\frac{w_{fg}}{\omega_f^2 - \omega_{fg}^2}\right). \tag{47}$$

Since $\omega_f > |\omega_{fg}|$, we have $\omega_f^2 - \omega_{fg}^2 > 0$ and the condition $D_f > |D_{fg}|$ can be expressed in terms of $\omega_f$ and $\omega_{fg}$ as

$$\omega_f^2 - 2\omega_f + 2|\omega_{fg}| - \omega_{fg}^2 < 0. \tag{48}$$

This relation can be easily solved for $\omega_f$ and we obtain the conditions

$$\begin{aligned} &\omega_{fg} < \omega_f < 2 - \omega_{fg}, \quad \text{if } \omega_{fg} > 0, \\ &-\omega_{fg} < \omega_f < 2 + \omega_{fg}, \quad \text{if } \omega_{fg} < 0. \end{aligned} \tag{49}$$

Since $\omega_f > 0$, condition (49) imposes that $|\omega_{fg}| < 1$. In the case where $\omega_{fg} = 0$, we recover the general condition $0 < \omega_f < 2$. The presence of the coupling between the two species therefore reduces the range of acceptable $\omega_f$ by $|\omega_{fg}|$ on both sides of the interval. The $\omega$-domain defined by Eq. (49) and representing the physical restriction $D_f > |D_{fg}|$ is illustrated in Fig. 4.

The numerical stability of the lattice Boltzmann algorithm was tested by scanning the region given by Eq. (49) for all permitted values of $\omega_{fg}$ and $\omega_f$, with a resolution of 0.01 for $\omega_f$ and 0.1 for $\omega_{fg}$. For each of these values, the eigenvalues of $\mathbf{P_k}$ have been computed numerically, for all wave vectors with $k_x = k_y$, $0 \leqslant k_x \leqslant 2\pi$. None of these eigenvalues have been found to be greater than 1. This shows that for this particular choice of diffusion matrix, the lattice Boltzmann multicomponent diffusion model is unconditionally stable.

To compare the stability field of the present LB method against finite-differences (FD), we discretize Eq. (1) to second order in space, setting the timestep $\delta t$ and gridspacing $\delta x$ to unity and simplifying the notation by omitting the spatial or temporal dependence of the variable when not necessary. Eq. (1) becomes

$$C(t+1) - C(t) = \mathcal{D}\begin{pmatrix} C_1(x+1,y) + C_1(x-1,y) + C_1(x,y+1) + C_1(x,y-1) - 4C_1 \\ C_2(x+1,y) + C_2(x-1,y) + C_2(x,y+1) + C_2(x,y-1) - 4C_2 \end{pmatrix}, \tag{50}$$

were $C$ is a vector with two components, $C_1$ and $C_2$. Taking the Fourier transform of this equation, we obtain the dispersion relation for the FD scheme

$$\exp(i\omega_\pm) = 1 + 2(\cos(k_x) + \cos(k_y) - 2)\lambda_\pm. \tag{51}$$

$\lambda_\pm$ are the eigenvalues of $\mathcal{D}$ given by Eq. (41).

The stability of the FD scheme requires $-1 < \exp(i\omega_\pm) \leqslant 1$, thus

$$0 \leqslant \lambda_\pm < \frac{1}{4}. \tag{52}$$

The above relation introduces constraints on the possible values of the diffusion coefficients. For the case we consider here in more detail, namely $D_f = D_g$ and $D_{fg} = D_{gf}$, the stability of the FD scheme requires

$$0 \leqslant D_f \pm D_{fg} < \frac{1}{4}. \tag{53}$$

In order to compare this range of stability with that of our LB model, we express the limits (53) in the space of the relaxation frequencies $\omega_f$ and $\omega_{fg}$, using Eqs. (44) and (45).

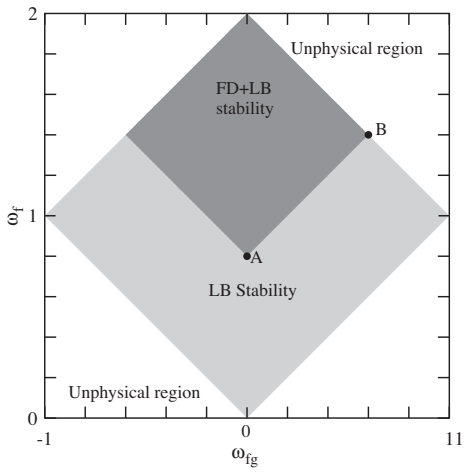


**Fig. 4.** The stability region of the lattice Boltzmann (LB) method for a symmetric diffusion matrix $\mathcal{D}$, with $D_{11} = D_{22} > 0$ and $D_{fg} = D_{gf}$ is shown in light gray shaded area. It spans the entire physical domains of acceptable diffusion coefficients. The finite difference method (FD) is only stable in the dark gray region. The white area is physically meaningless as it corresponds to a negative diffusion. Points $A$ and $B$ are: $A = (0, 4e_s^2/(1+2e_s^2))$, $B = (1/(1+2e_s^2), (1+4e_s^2)/(1+2e_s^2))$. In the figure, we choose $e_s^2 = 1/3$.

The stability region (53) is shown as a dark shaded area on Fig. 4. Note that the stability of the FD scheme was tested numerically and found to be in perfect agreement with Eq. (52). The FD scheme has a narrower region of stability than our LB model, at least for this particular case. The stability regions of the two algorithms can be tested analogously for other choices of diffusion matrices (non-symmetric ones and/or with $D_f \neq D_g$) but generalizing is beyond the scope of the present study.

## 4. Lattice Boltzmann model for advection and coupled diffusion

Advection–diffusion models developed with the lattice Boltzmann method have been used to solve a wide variety of problems over the last decade, from thermo-hydrodynamics to reaction in porous media [21,19]. The method we use here is based on the multiple distribution model [33,14,4], where the hydrodynamics is solved by a conventional BGK equation [30] on a D2Q9 lattice with nine velocity vectors $\mathbf{c}_i$ (connecting nearest and second nearest neighbors, and with $\mathbf{c}_0 = 0$)

$$f_i(\mathbf{x}+\mathbf{c}_i, t+1) = (1-\omega_f) f_i(\mathbf{x}, t) + \omega_f f_i^0(\mathbf{x}, t). \tag{54}$$

The equilibrium distribution $f_i^0$ for the flow field is now given by [30]

$$f_i^0 = \rho t_i^* \left(1 + 3\mathbf{u}\cdot\mathbf{c}_i + \frac{9}{2}(\mathbf{u}\cdot\mathbf{c}_i)^2 - \frac{3}{2}\mathbf{u}\cdot\mathbf{u}\right), \tag{55}$$

where the weights are $t_0^* = 16/36$, $t_i^* = 4/36$ for $i = 1, 2, 3, 4$ and $t_i^* = 1/36$ for $i = 5, 6, 7, 8$ and $\rho$ is the local value of the density field. The density and momentum are obtained through the first two moments of the distribution $f_i$

$$\rho = \sum_i f_i = \sum_i f_i^0, \quad \rho\mathbf{u} = \sum_i f_i \mathbf{c}_\mathbf{i} = \sum_i f_i^0 \mathbf{c}_\mathbf{i}. \tag{56}$$

In this model, the kinematic viscosity $\nu$ and pressure $p$ are given by

$$\nu = \frac{1}{3}\left(\frac{1}{\omega_f} - \frac{1}{2}\right), \quad p = \frac{1}{3}\rho. \tag{57}$$

The advection–diffusion equations for each of the $p$ diffusing components are described by the set of $p$ equations

$$g_i^p(\mathbf{x}+\mathbf{e}_\mathbf{i}, t+1) = (1-\omega_p) g_i^p(\mathbf{x}, t) + \omega_p g_i^{p0}(\mathbf{x}, t). \tag{58}$$

The multiple distribution method permits different lattice topologies for the different sets of distributions. While we use a D2Q9 lattice for $f_i$, a D2Q5 topology (with $\mathbf{e}_0 = 0$) is sufficient for the $g_i^p$. The distributions $f_i$ and $g_i^p$ are coupled through the equilibrium distribution $g_i^{p0}$, which now becomes

$$g_i^{p0} = C_p t_i (1 + 3\mathbf{u}\cdot\mathbf{e}_i + \mathcal{O}(u^2)). \tag{59}$$

For D2Q5, the weights $t_i$ are again 1/3 and 1/6, respectively for $i = 0$ and $i \neq 0$, $e_s^2 = 1/3$. The local concentration of component $p$ is $C_p$ and $\mathbf{u}$ is the local velocity field, as obtained from Eqs. (54) and (56). The choice of an equilibrium distribution depending linearly on the macroscopic field is common but introduces a numerical diffusivity that depends quadratically on the velocity $\mathbf{u}$ [11,32,4]. In all following calculations, the Mach number is everywhere $\ll 1$ so that this effect is expected to be negligible.

As in the previous section, the diffusivity for component $p$ is found to be

$$D_{pp} = \frac{1}{3}\left(\frac{1}{\omega_p} - \frac{1}{2}\right). \tag{60}$$

We modify the BGK dynamics of Eq. (58) to include the extra non-diagonal diffusive terms in a procedure similar to that presented in Section 3. The new BGK equations for the evolution of the distributions $g_i^p$ become

$$g_i^p(\mathbf{x}+\mathbf{e}_\mathbf{i}, t+1) = (1-\omega_p) g_i^p(\mathbf{x}, t) + \omega_p g_i^{p0}(\mathbf{x}, t) - \sum_{k\neq p} \omega_{pk}\left(\bar{g}_i^{k0}(\mathbf{x}, t) - g_i^k(\mathbf{x}, t)\right), \tag{61}$$

where the equilibrium distribution for the non-diagonal terms $\bar{g}_i^{k0}$ are given by the equilibrium distribution defined in Eq. (9). It can be shown by a Chapman–Enskog expansion that, at low Mach number, Eqs. (61) and (54) lead to the following set of macroscopic equations

$$\begin{aligned} &\frac{\partial \mathbf{u}}{\partial t} + (\mathbf{u}\cdot\nabla)\mathbf{u} = -\frac{1}{\rho}\nabla p + \nu\nabla^2\mathbf{u}, \\ &\frac{\partial C_p}{\partial t} + \mathbf{u}\cdot\nabla C_p = D_{pp}\nabla^2 C_p + \sum_{k\neq p} D_{pk}\nabla^2 C_k \end{aligned} \tag{62}$$

with the diffusion matrix $D_{kl}$ given by Eq. (24).

The present LBGK model for multicomponent diffusion can be modified to incorporate some features that improve accuracy. Ginzburg [11] presents an approach based on the equilibrium distribution model (E-model). In the context of the two relaxation time (TRT) collision operator, the two eigenvalues can be chosen to optimize the accuracy of the model, cancel numerical diffusion and reduce higher order correction terms. However, for the D2Q5 lattice we use in this study, the lack of diagonal velocity distribution does not allow us to cancel cross-diagonal terms of numerical diffusion [32]. Servan-Camas and Tsai [32] showed, however, that using pseudo-velocities the numerical diffusivity of the scheme can be reduced from first to second order in time. An in depth analysis of numerical diffusion is not within the scope of this study, but the two approaches proposed by Ginzburg [11] and Servan-Camas and Tsai [32] can be implemented for any choice of collision operator including the model presented here.

### 4.1. Boundary conditions

In the next section we will present some applications of our model. These applications require us to define proper boundary conditions at the limit of the computational domain. For the sake of illustration, we have only implemented basic boundary conditions that we briefly describe below. Our multicomponent diffusion LBGK model is compatible with more sophisticated boundary conditions.

In Section 5.3, the upper boundary condition for the advected scalar fields is a prescribed concentration for sodium (Na). We implement this Dirichlet boundary condition by setting the unknown distribution $g_4$ at the boundary node

$$g_4(\text{wall}) = C(\text{wall}) - \sum_{j\neq 4} g_j(\text{wall}). \tag{63}$$

The constant flux $\nabla_n \mathbf{J} = 0$ normal to boundary at the inlet and outlet of the domain in Section 5.2 are set by a finite difference approximation for the gradient of the concentration obtained by the non-equilibrium part of the distributions $g$'s (Eq. (5)).

Otherwise, we use a standard bounce-back condition at solid–liquid boundaries to ensure no-slip boundary conditions for the hydrodynamic distributions $f_i$ and for the zero normal flux condition on solid boundaries for the diffusing species ($g_i$). This choice of boundary condition offers the advantage of simplicity, however it carries several disadvantages. First, it constrains the position of the solid–liquid interface to be halfway between the nodes, a condition that is not generally respected in the case of boundaries not aligned with the axis of the lattice. The second issue associated with our choice of boundary conditions (bounce-back for the zero normal flux for the scalar fields) is problematic for the tangential part of the flux. As noted by Drazer and Koplik [5], Zhang et al. [39] and Ginzburg [12], the bounce-back of the incoming distribution at a boundary results in a zero tangential flux condition which is not physical because of the allowed diffusive flux along the boundary. Nevertheless, the bounce-back of a scalar field (for example temperature) has been used extensively for adiabatic boundary conditions [22,36,37].

The treatment of boundary conditions in a more sophisticated way to correct for the inaccuracy of the effective wall position is independent of the scheme that we present here as the model can be used to implement any type of boundary conditions. For instance, the model presented in this study (summarized in Eq. (6)) can be generalized to be compatible with the multi-reflection condition for the anti-symmetric part of the equilibrium distributions developed by Ginzburg [12] to allow for a better treatment of the tangential flux condition along a solid boundary. The implementation of the boundary conditions presented in Ginzburg [12] does not depend on the choice of collision operator and therefore can be readily included in the present multicomponent advection–diffusion model.

The scope of this study is to present a new, straight-forward algorithm to solve for multicomponent coupled diffusion. The goal of Sections 5.2 and 5.3 is to illustrate the potential of the method for advection–diffusion problems.

## 5. Results

### 5.1. Diffusion coupling in one dimension

We first validate the results obtained with our lattice Boltzmann model without advection. We model the simple case where two components $C_1$ and $C_2$ diffuse. $C_1$ is coupled to $C_2$ via a finite diffusivity $D_{12}$ ($D_{21} = 0$). We compare our results to those obtained with an explicit finite-difference code. We use a grid with 50 nodes, grid spacing $dx = 1/50$, time step $dt = 10^{-6}$. The left and right boundaries have fixed concentrations. An excellent agreement is found between the two methods over a wide range of $D_{12}$ (see Fig. 5(a)–(c)). For example the two tests shown in Fig. 5(a) and (b) correspond to ratios of maximum diagonal versus non-diagonal diffusivities ($D_{ii}^{max}/D_{ij},\ i \neq j$) of 0.5 and 10, respectively. Note that when $D_{21} = 0$, Eq. (41) shows that the two eigenvalues are $D_{11}$ and $D_{22}$ and then Eq. (52) does not set limits on the ratio $D_{ii}/D_{ij}$.

The model was also tested successfully for the case where $\omega_{12} < 0$, to model an opposite coupling that can arise, for example, in the case of the diffusion of two oppositely charged constituents under the requirement of local charge conservation (see Fig. 5(c)).

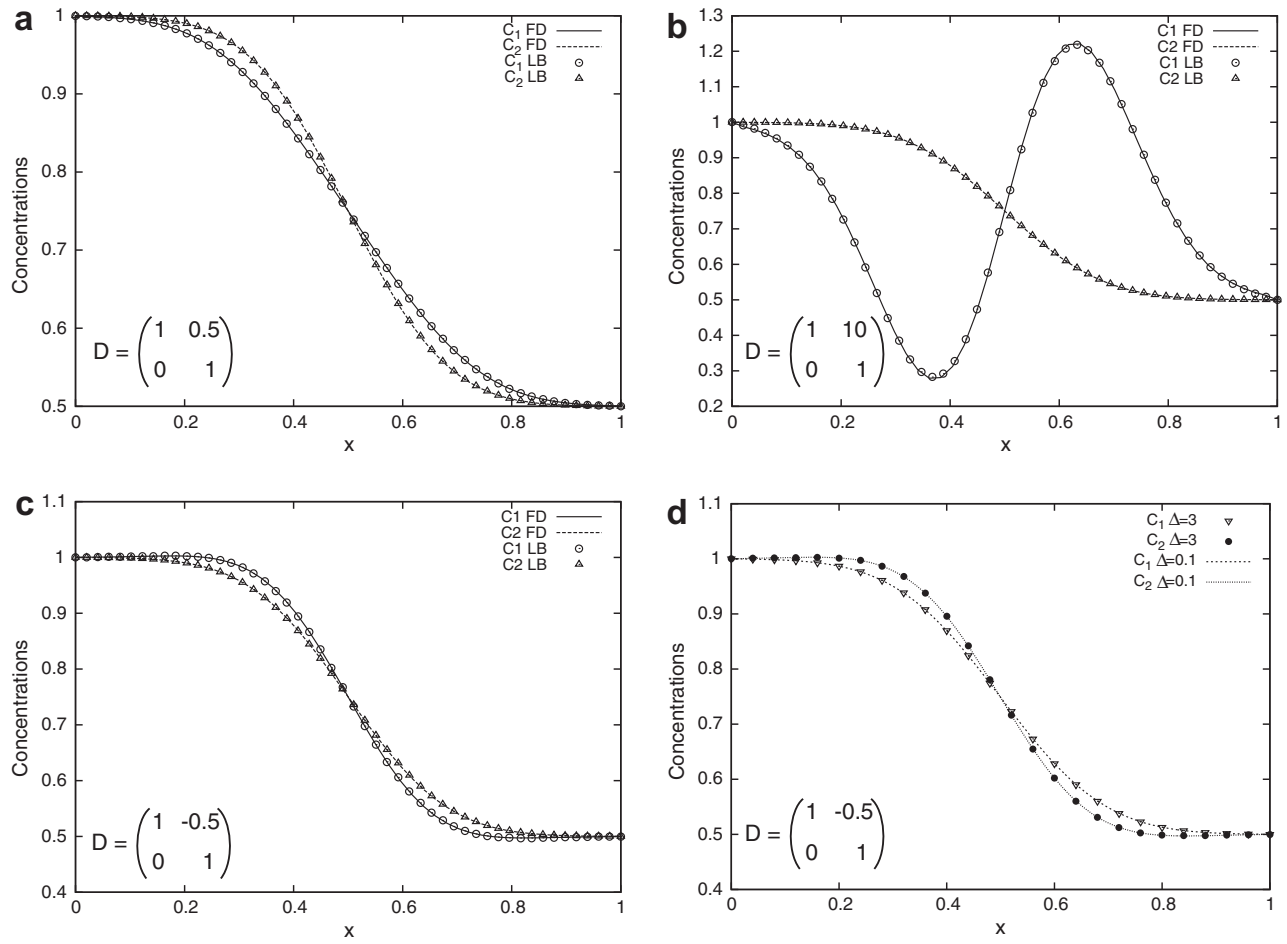


**Fig. 5.** Comparison between calculation with a simple explicit finite-difference scheme (FD) and the lattice Boltzmann model (LB) developed here. (a) The non-diagonal term of the diffusion matrix is half the magnitude of the diagonal terms. (b) The non-diagonal term of the diffusion matrix is an order of magnitude higher than the diagonal terms. (c) The non-diagonal term of the diffusion matrix $D_{12} = -0.5 \times D_{11} = -0.5 \times D_{22}$. (d) Same as for (c) but for two different diffusion numbers $\Delta = D_{11}dt/dx^2$. Finite difference explicit methods are only stable for $\Delta < 1/4$, our model has shown no instability for all the test problems we have considered.

### 5.2. Coupled advection and diffusion in complex geometries

The problem of the flow of a solution along a reactive surface has a wide variety of applications especially in biology and geosciences. In water, dissolved salts are found in the form of charged ions and their transport can be coupled because of local charge conservation or because they diffuse as compounds. Felmy and Weare [8,9] studied the case of sodium diffusing from a salt diapir into motionless seawater (no advection). They investigated the effects of the non-diagonal couplings of the diffusion matrix for the system $Na^+$, $K^+$, $Ca^{2+}$, $Mg^{2+}$ and $SO_4^{2-}$, where they use the diffusivities listed in Table 1.

We illustrate the possibilities offered by this new lattice Boltzmann scheme with a simple example of coupled diffusion in a porous medium in two dimensions.

We compare results for different Peclet numbers ($u_D d/D_{Na}$, where $u_D$ is the Darcy velocity, $d$ is the diameter of the solid particles in the porous medium) and show the conjugate effects of dispersion and coupled diffusion in the distribution of ions from an initial circular source. Again, we neglect the dependence of the diffusivities on the concentration of the different

**Table 1**
Diffusion matrix for Na, K, Ca, Mg and $SO_4$ in seawater in $10^{-5}$ cm$^2$/s. $J_p$ represents the flux of component $p$. From Felmy and Weare [8,9], Ingebritsen and Sanford [20].

| | ∇Na | ∇K | ∇Ca | ∇Mg | ∇$SO_4$ |
|---|---|---|---|---|---|
| $J_{Na}$ | 1.398 | 0.015 | 0.729 | 0.805 | −0.754 |
| $J_K$ | 0.007 | 1.793 | 0.023 | 0.026 | −0.037 |
| $J_{Ca}$ | 0.007 | 0.002 | 0.604 | 0.023 | −0.046 |
| $J_{Mg}$ | 0.023 | 0.008 | 0.076 | 0.575 | −0.108 |
| $J_{SO_4}$ | −0.015 | −0.026 | −0.16 | −0.113 | 0.833 |

components. The problem we use is inspired from the problem studied by Felmy and Weare [8,9]. However, we allow seawater to flow (from left to right) because of a fixed pressure gradient. We initially set a circular pocket of a solution ten times more concentrated in Na than the seawater at the center of the domain (same concentration for the other components). The geometry of the problem is illustrated in Fig. 6.

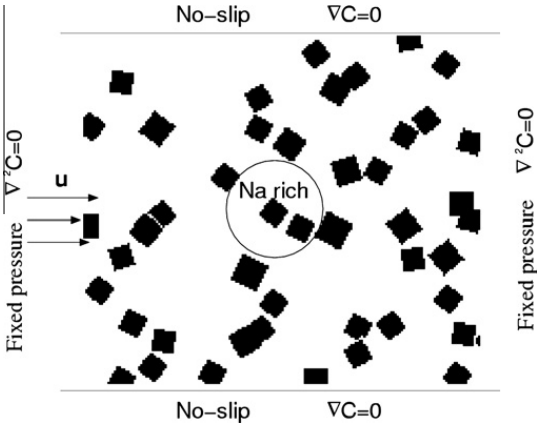


**Fig. 6.** Set-up for the advection-coupled diffusion calculations. The grid used in the calculations is 200 by 163.

**Table 2**
Molarities used for the calculations. From Felmy and Weare [8,9], Ingebritsen and Sanford [20].

| | Na | K | Ca | Mg | $SO_4$ |
|---|---|---|---|---|---|
| Na-rich solution | 5.305 | 0.0106 | 0.0107 | 0.055 | 0.0293 |
| Seawater | 0.5 | 0.0106 | 0.0107 | 0.055 | 0.0293 |

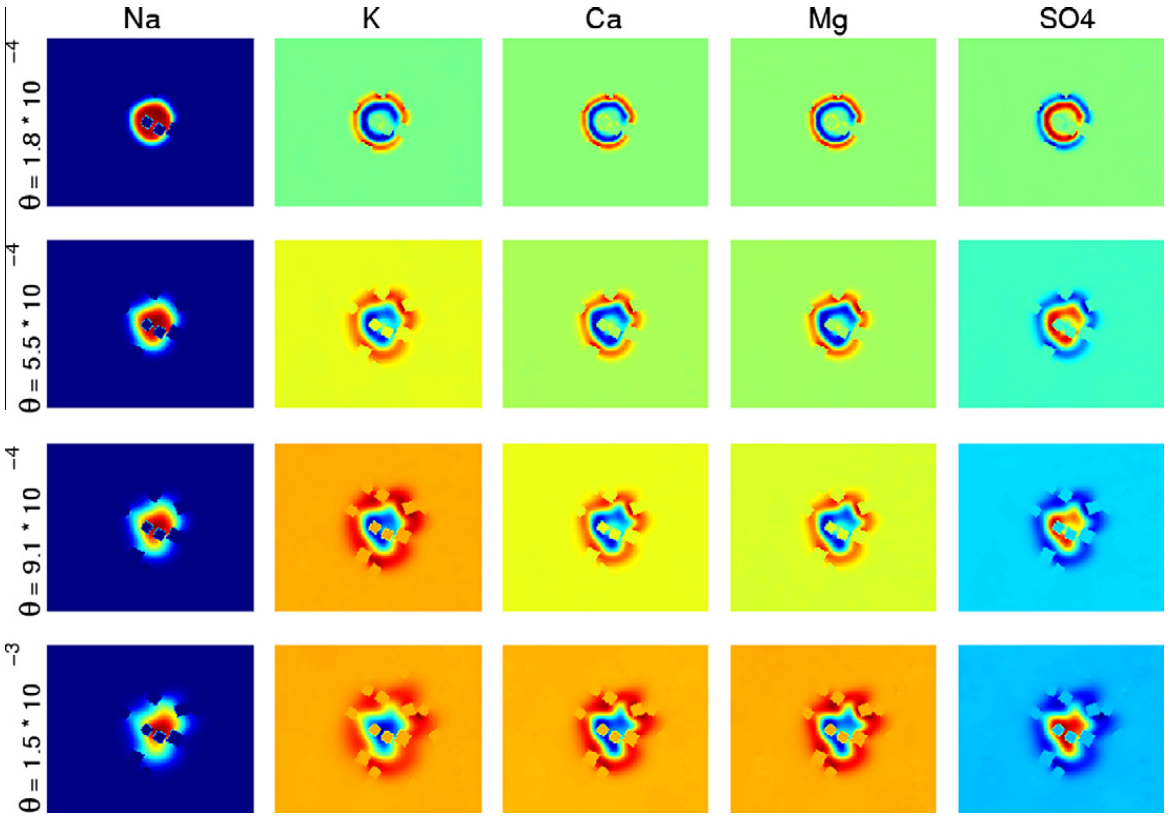


**Fig. 7.** Concentration of the different ions for Pe = 0.322 at four different dimensionless times ($\theta = D_{Na}t/L^2$). See the text for more details.

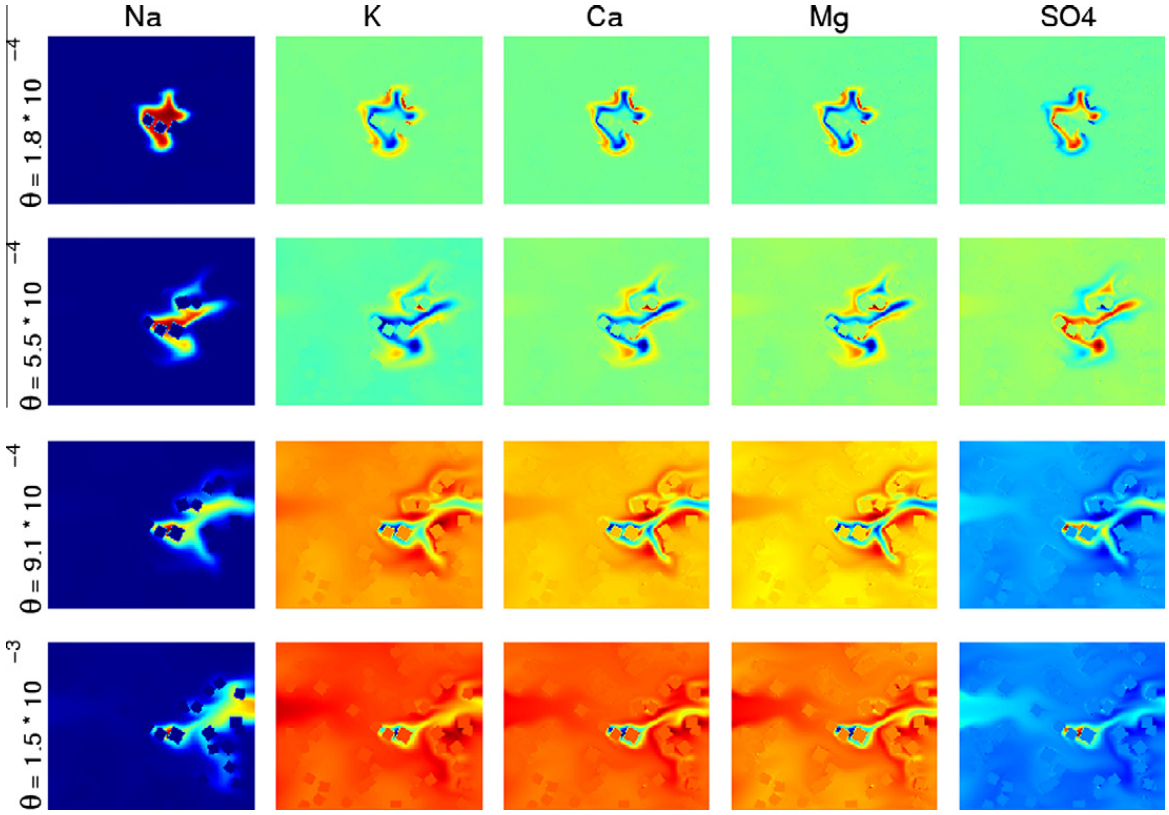


**Fig. 8.** Concentration of the different ions for Pe = 3.22 at four different dimensionless times ($\theta = D_{Na}t/L^2$). See the text for more details.

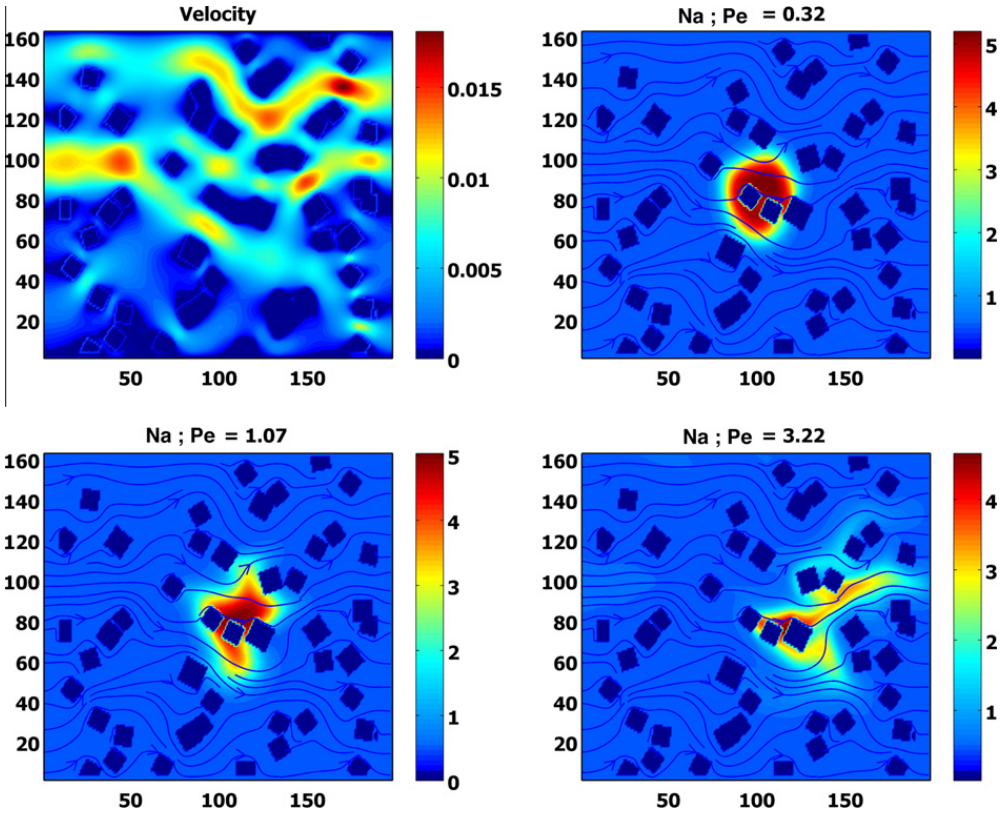


**Fig. 9.** Magnitude of the velocity field (upper left), and Na concentrations (with superposed streamlines) for Pe = 0.322, 1.07 and 3.22 at dimensionless time $\theta = D_{Na}t/L^2 = 7.3 \times 10^{-4}$.

The upper and lower boundary conditions are set to no-slip and no-flux with respect to concentration. The no-slip boundary conditions on the solid matrix, upper and lower boundaries are obtained by a bounce-back of the density distributions. The left and right boundaries are fixed to a constant flux with respect to concentrations. For the fluid, the right boundary condition is a fixed pressure, lower than the left side to set up a small pressure gradient and consequently a flow from left to right. The pressure gradient is set-up so that the Reynolds number (ratio of inertial forces over viscous forces) is smaller than 1 (about $10^{-1}$ for the porous media flow). The initial concentrations are given in Table 2. The calculations are performed

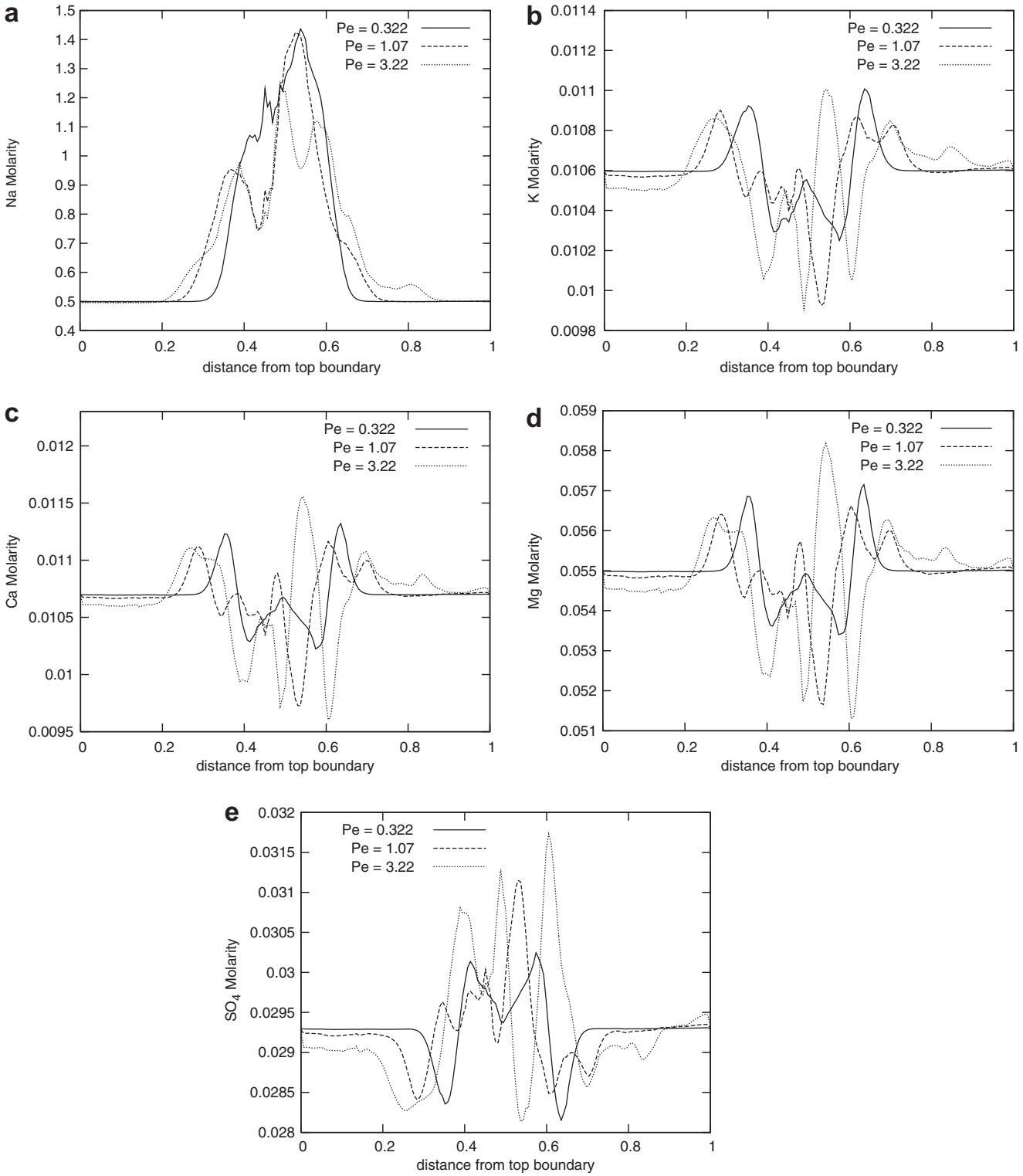


**Fig. 10.** Concentration profiles (averaged horizontally) of the different ions for Pe = 0.322, 1.07 and 3.22 at $\theta = D_{Na}t/L^2 = 7.3 \times 10^{-4}$. See the text for more details.

on a grid of 200 × 163 nodes. The results are shown in Fig. 7 for Pe = 0.322 and Fig. 8 for Pe = 3.22. The solid fraction in the porous media is assumed to be inert with respect to diffusion reflecting the difference of timescales between diffusion in a solid and in a solution (several orders of magnitude). Each column shows the concentration of a different ion at four different dimensionless times $\theta$ (where $\theta = D_{Na}t/L^2$, $L$ is the horizontal length of the computational domain). As the initial Na-rich circular region and the seawater had the same initial concentrations for K, Ca, Mg and $SO_4$, the variations of concentration for these ions are the consequence of the non-diagonal terms of the diffusion matrix (the coupling with Na). It is also important to note that due to coupling, the distribution of every cation is positively correlated to Na and $SO_4$ is anti-correlated as expected from charge balance (element of diffusion matrix with opposite sign).

Fig. 8 shows the same temporal evolution for Pe = 3.22. The distribution of ions extends over a broader region and as expected from the increased contribution of advection, the approximate radial symmetry observed for Pe = 0.322 is broken. Fig. 9 allows us to better appreciate the importance of the Peclet number in the distribution of Na, showing the flow field and the Na concentrations at the same dimensionless time ($\theta = 7.3 \times 10^{-4}$) for three different Peclet numbers (0.322, 1.07 and 3.22). The streamlines of the flow field are superposed on the concentrations to show that the concentration becomes better correlated with the flow field as the Peclet number increases.

Fig. 10 shows the horizontally-averaged vertical profiles of concentrations for each ion for Pe = 0.322, 1.07 and 3.22 at $\theta = 7.3 \times 10^{-4}$. Although the overall direction of the flow field set-up by the imposed pressure gradient is perpendicular to the profiles, dispersion effects due to the tortuosity of the flow paths around the solid particles are responsible for the wider distribution of Na observed for Pe = 3.22. $SO_4$ is again anti- correlated with the cations. The complexity of the profiles is due to the complexity of the dispersion effect due to the solid particles, which act both as an insulating boundary condition for the different ions and disturbs the flow field.

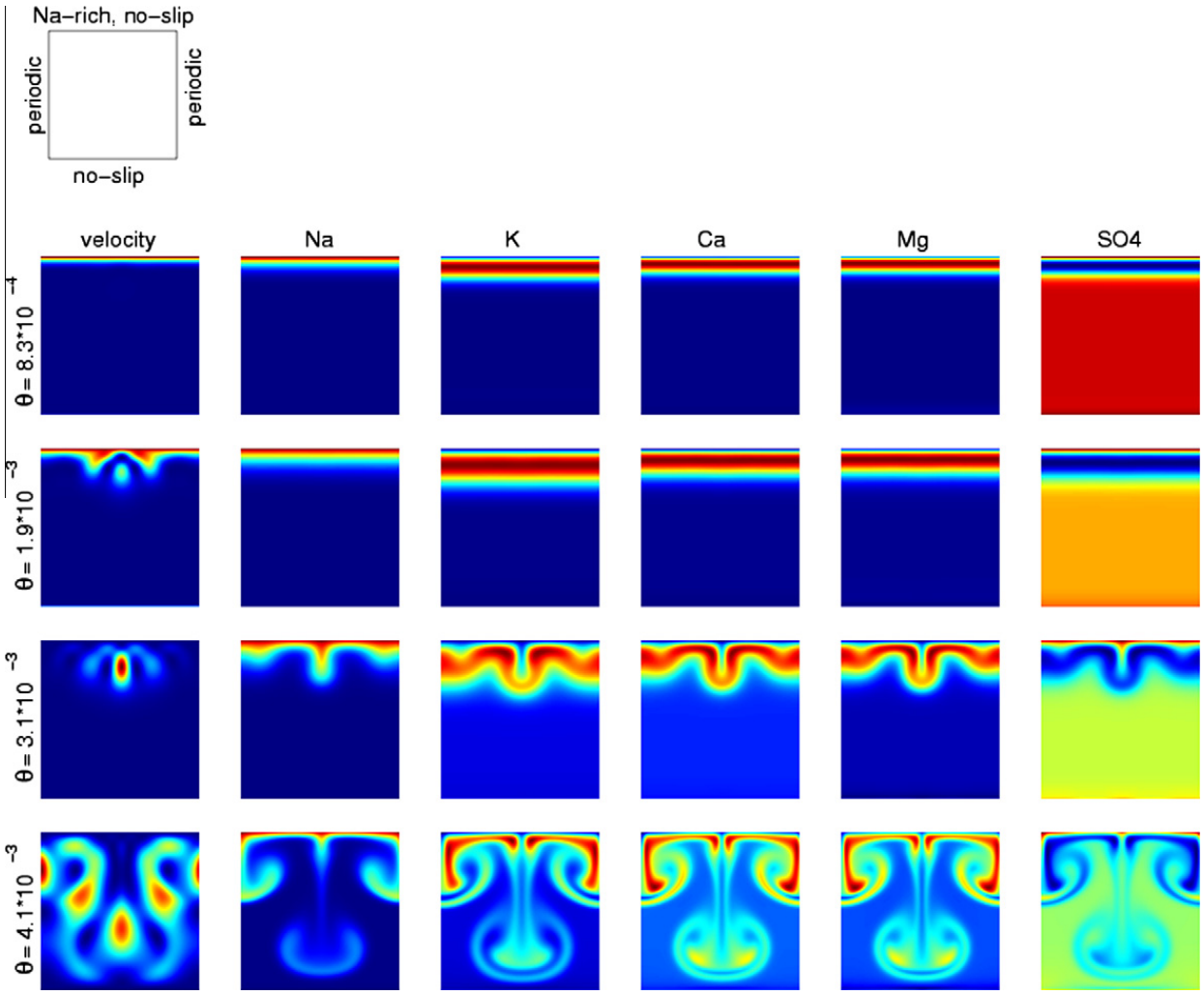


**Fig. 11.** Convection due to concentration differences. The upper plot illustrates the set-up of the simulation. As for the previous calculations, Na is the only component with any initial gradient in concentration. The buoyancy force is linearly proportional to the amount of salt dissolved (see text for more details). The evolution of the system is shown for four different dimensionless times $\theta = D_{Na}t/L_y$, where $L_y$ is now the vertical dimension of the computational domain.

### 5.3. Coupled convection and diffusion

In the case of seawater in contact with a salt diapir (NaCl), the dissolution and transport of dissolved Na from the boundary increases the density of the solution and can lead to compositional convection (where the buoyancy is due to composition differences). Here, we investigate the effect of coupled diffusion on haline convection and the evolution of the distribution of different ions dissolved in seawater. As for the previous example, Na is the only ion with an initial gradient. We set the composition of the salt diapir equal to the composition of the Na-rich pocket of solution, as in the previous section (see Table 2). The fluid is initially at rest. The dissolution of NaCl and redistribution of ions lead to a buoyancy force

$$\Delta\rho\mathbf{g} = \rho_0\mathbf{g}\sum_k m_k\left(C_k - C_k^{sw}\right), \tag{64}$$

where $\rho_0$ is the density of seawater, $\mathbf{g}$ is the acceleration due to gravity, $m_k$ is the molar mass fraction of the component $k$ and $(C_k - C_k^{sw})$ is the concentration difference of ion $k$ between the solution and seawater. As $Na^+$ is the only ion with an initial gradient, we define the Rayleigh number in this case by

$$Ra_{Na} = \frac{\Delta\rho_{Na} g L_y^3}{\mu D_{Na}}. \tag{65}$$

$\Delta\rho_{Na}$ is the density difference due only to Na, $L_y$ is the vertical dimension of the computational domain, $\mu$ is the dynamic viscosity of seawater (here assumed constant) and $D_{Na}$ the diagonal component of the diffusion matrix for Na.

Fig. 11 shows the set-up for the calculation (top) and the velocity and concentration distributions at four different dimensionless times $\theta = D_{Na}t/L_y^2$. The Rayleigh number for this calculation is about $2.9 \times 10^6$. Again, diffusive coupling between the different ions and Na is responsible for the redistribution of K, Ca, Mg and $SO_4$. K, Ca and Mg are concentrated ahead of the Na diffusion front, where Na gradients are the largest. The negative correlation between $Na^+$ and $SO_4^{2-}$ is again clearly observable.

## 6. Conclusions

Multiple component diffusion is ubiquitous in most transport processes. When the different diffusing species interact (through their charge for ions, or as compounds–molecules) the diffusion problem becomes more complicated because of the coupling that arises between the different species. These couplings lead to non-diagonal terms in the diffusion matrix that can be significant in the transport of components and properties of the diffusing media (rheology, electrical conductivity to cite a few).

We present a new lattice Boltzmann (LB) method that includes the effect of diffusion coupling in both diffusion and advection–diffusion problems. We first analyzed this new model in a theoretical way, discussing its stability and accuracy. With both a Chapman–Enskog expansion and an investigation of the eigenvalue of the LB evolution operator, we showed that, up to derivatives of order higher than two, our model reproduces multicomponent diffusion. Unconditional numerical stability has been demonstrated for a particular class of diffusion matrices. Numerical experiments suggests that stability is probably maintained in more general situations. However, with advection we showed that we may no longer expect unconditional stability.

In a second step, we tested numerically the model for several applications. For the diffusion of two coupled components in one dimension, we compared our results with an explicit finite difference code. The results are in excellent agreement for a wide range of the ratio $D_{ii}^{max}/D_{ij}$, with $(i \neq j)$.

We then apply the advection–diffusion model to the problem of flow in a porous medium where we introduce a circular Na-rich region in the solution (seawater). Although the solution (seawater) and the Na-rich region are initially at equilibrium with respect to the other diffusing species, their coupling with Na drives them out of equilibrium and results in regions with high concentrations in K, Ca, Mg and $SO_4$. The $SO_4$ anion has an opposite charge and because of charge conservation (negative coupling), its distribution becomes anti-correlated with the distribution of the other ions. This example illustrates the potential of this model to solve coupled diffusion problems with fluid flow in complex geometries in a straight-forward way.

## Acknowledgements

We would like to thank three anonymous reviewers and the editor for insightful reviews. C.H. and M.M. were funded by NSF EAR 0608885. B.C. was funded by the Swiss National Fund for Sciences.

## Appendix A. Stability of the single component diffusion model – "Energy" approach

In this section we prove the stability of the lattice Boltzmann BGK model (LBGK) for the diffusion of a single component. Our approach is based on the conservation of a positive-defined function reminiscent of an energy. To simplify the notation, we rewrite Eq. (2) as

$$f_i^{out} = f_i + \frac{1}{\tau}\left(f_i^{eq} - f_i\right), \tag{A.1}$$

where $f^{out}$ denotes the post collision distribution functions and $f = f^{in}$ the pre-collision ones, $\tau = 1/\omega$ and

$$f_i^{eq} = t_i C, \quad C = \sum_i f_i. \tag{A.2}$$

The lattice weights are positive and obey again

$$\sum_i t_i = 1, \quad \sum_i t_i v_{i\alpha} v_{i\beta} = c_s^2 \delta_{\alpha\beta}. \tag{A.3}$$

It is well known that the LBGK diffusion model predicts a diffusion coefficient

$$D = \delta_t c_s^2 \left(\tau - \frac{1}{2}\right).$$

Using Eq. (A.2), the LBGK equation reads

$$f_i^{out} = \frac{t_i}{\tau} C + \left(1 - \frac{1}{\tau}\right) f_i. \tag{A.4}$$

We assume that the lattice weights are all identical for $i \neq 0$

$$t_i = t, \quad \text{if } i \neq 0. \tag{A.5}$$

Therefore we have

$$\sum_i t_i = t_0 + zt = 1, \tag{A.6}$$

where $z$ is the lattice coordination number, i.e. the number of non-zero velocities.

We define an "energy" $E$ as

$$E = \begin{cases} \frac{t}{t_0} (f_0)^2 + \sum_{i \geqslant 1} (f_i)^2, & \text{if } t_0 \neq 0, \\ \sum_{i \geqslant 1} (f_i)^2, & \text{if } t_0 = 0. \end{cases} \tag{A.7}$$

From Eq. (A.4) we can now compute (for the case $t_0 \neq 0$)

$$\begin{aligned} E^{out} &= \frac{t}{t_0} \left(f_0^{out}\right)^2 + \sum_{i \geqslant 1} \left(f_i^{out}\right)^2 \\ &= \frac{t}{t_0} \left[\frac{t_0^2}{\tau^2} C^2 + 2 \frac{t_0}{\tau} \left(1 - \frac{1}{\tau}\right) C f_0 + \left(1 - \frac{1}{\tau}\right)^2 f_0^2\right] + \sum_{i \geqslant 1} \left[\frac{t^2}{\tau^2} C^2 + \frac{2t}{\tau} \left(1 - \frac{1}{\tau}\right) C f_i + \left(1 - \frac{1}{\tau}\right)^2 f_i^2\right] \\ &= \left(1 - \frac{1}{\tau}\right)^2 \left[\frac{t}{t_0} f_0^2 + \sum_{i \geqslant 1} f_i^2\right] + \left(\frac{t t_0}{\tau^2} + z \frac{t^2}{\tau^2}\right) C^2 + 2 \frac{t}{\tau} \left(1 - \frac{1}{\tau}\right) C f_0 + 2 \frac{t}{\tau} \left(1 - \frac{1}{\tau}\right) C \sum_{i \geqslant 0} f_i. \end{aligned} \tag{A.8}$$

Recalling that

$$\sum_{i \geqslant 1} f_i = C - f_0,$$

we can write

$$E^{out} = \left(1 - \frac{1}{\tau}\right)^2 E^{in} + \frac{t}{\tau^2} (t_0 + zt + 2\tau - 2) C^2 + 2 \frac{t}{\tau} \left(1 - \frac{1}{\tau}\right) C f_0 - 2 \frac{t}{\tau} \left(1 - \frac{1}{\tau}\right) C f_0. \tag{A.9}$$

With $t_0 + zt = 1$ we finally obtain

$$E^{out} = \left(1 - \frac{1}{\tau}\right)^2 E^{in} + \frac{t}{\tau^2} (2\tau - 1) C^2. \tag{A.10}$$

Eq. (A.10) is also satisfied in a model without a rest population, when $t_0 = 0$ and $f_0 = 0$.

We also observe that

$$1 - \left(1 - \frac{1}{\tau}\right)^2 = 1 - \left(1 - \frac{2}{\tau} + \frac{1}{\tau^2}\right) = \frac{2}{\tau} - \frac{1}{\tau^2} = \frac{2\tau - 1}{\tau^2}.$$

Therefore Eq. (A.10) becomes

$$E^{out} = \left(1 - \frac{1}{\tau}\right)^2 E^{in} + t \left[1 - \left(1 - \frac{1}{\tau}\right)^2 C^2\right]. \tag{A.11}$$

Since $C$ is conserved by the collision rule, we have

$$C^{out} = C^{in}$$

and Eq. (A.11) can be written as

$$S^{out} \equiv E^{out} - t(C^{out})^2 = \left(1 - \frac{1}{\tau}\right)^2 [E^{in} - t(C^{in})^2] \equiv \left(1 - \frac{1}{\tau}\right)^2 S^{in}. \tag{A.12}$$

We note that the conservation law (A.12) is only obeyed for a lattice satisfying Eq. (A.6).

For $1/2 \leqslant \tau < \infty$, we have

$$\left(1 - \frac{1}{\tau}\right)^2 \leqslant 1. \tag{A.13}$$

Below we will show that $S$ cannot be negative, for any values of the $f_i$'s. For now let us assume that $S \geqslant 0$. Then Eqs. (A.12) and (A.13) impose

$$E^{out} - tC^2 \leqslant E^{in} - tC^2.$$

Thus $E^{out} \leqslant E^{in}$ and the $f$'s are bound and the method is unconditionally stable for every choice of relaxation time $\tau > 1/2$.

Let us now show that

$$S \equiv E - tC^2 = \frac{t}{t_0} f_0^2 + \sum_{i>0} f_i^2 - t \sum_{i,j} f_i f_j \geqslant 0, \tag{A.14}$$

for all values of $f$. We consider the case with and without rest particles.

### A.1. Lattices with no rest particles

For lattice topologies with no rest velocity (such as D2Q4, for example), we have $t = 1/z$ and $S$ reduces to

$$S = \sum_{i=1}^{z} f_i^2 - t \sum_{i,j=1}^{z} f_i f_j. \tag{A.15}$$

For any real values $f_i$ and $f_j$, we have

$$(f_i - f_j)^2 \geqslant 0 \tag{A.16}$$

and then

$$f_i f_j \leqslant \frac{1}{2}\left(f_i^2 + f_j^2\right). \tag{A.17}$$

Summing over all velocities twice (for $i$ and $j$) we get

$$\sum_{i,j=1}^{z} f_i f_j \leqslant \frac{z}{2}\left(\sum_{i=1}^{z} f_i^2 + \sum_{j=1}^{z} f_j^2\right). \tag{A.18}$$

Therefore,

$$\frac{1}{z} \sum_{i,j} f_i f_j \leqslant \sum_i f_i^2 \tag{A.19}$$

and, with $t = 1/z$, this shows that $S \geqslant 0$.

### A.2. Lattices with rest particles

Eq. (A.14) can be written as $S = \mathbf{f}^T \mathbf{A} \mathbf{f}$, where the matrix $\mathbf{A}$ is

$$\mathbf{A} = t \begin{pmatrix} \frac{1}{t_0} - 1 & -1 & \dots & -1 \\ -1 & \frac{1}{t} - 1 & \dots & -1 \\ \dots & \dots & \dots & \dots \\ -1 & \dots & -1 & \frac{1}{t} - 1 \end{pmatrix} \tag{A.20}$$

and the vectors $\mathbf{f}$ and $\mathbf{f}^T$ are respectively the vector containing the $z+1$ velocity distributions and its transpose. If $\mathbf{A}$ is a positive semi-definite matrix, i.e. $\mathbf{f}^T \mathbf{A} \mathbf{f} \geqslant 0$ for all choices of $f$'s, then $S \geqslant 0$ and the method is unconditionally stable for $\tau > 1/2$.

Since **A** is real and symmetric, it can be diagonalized and the condition $S \geqslant 0$ reduces to having all the eigenvalues of $\mathbf{A}\lambda_A \geqslant 0$.

For D2Q3, D2Q5, D2Q9 and D3Q7, the eigenvalues of **A** are found to be

$$\begin{aligned} &\lambda_1 = 1 \quad \text{with multiplicity } z-1, \\ &\lambda_\pm = \frac{t+t_0-(z+1)tt_0 \pm \sqrt{(t+t_0-(z+1)tt_0)^2 - 4t_0(-t+zt^2+tt_0)}}{2t_0}. \end{aligned} \tag{A.21}$$

Using $t_0 = 1 - zt$, $\lambda_-$ reduces to 0 and $\lambda_+$ to

$$\lambda_+ = 1 + \frac{t}{t_0} - (z+1)t.$$

To show that $\lambda_+$ is always positive we have to show that

$$\frac{1}{t} + \frac{1}{t_0} > z+1.$$

This is true because we always have $t < 1/z$ and $t_0 < 1$. Then, $1/t > z$ and $1/t_0 > 1$ and we prove the unconditional stability of the single component LBGK diffusion model.

## Appendix B. Loss of unconditional stability of the single component advection–diffusion model – "Energy" approach

The stability conditions for the single component advection–diffusion scheme have been investigated by Suga [35], Servan-Camas and Tsai [32]. In the following section, in the context of Appendix A, we illustrate the loss of unconditional stability. In this case, the different equilibrium distribution leads to an "energy" conservation equation with additional terms (compared to Eq. (A.12))

$$E^{out} - tC^2 = \left(1 - \frac{1}{\tau}\right)^2 (E^{in} - tC^2) + \frac{t}{\tau C_s^2}\rho[\rho u^2 + 2\left(1 - \frac{1}{\tau}\right)\mathbf{u}\cdot\mathbf{J}]. \tag{B.1}$$

The last two terms of Eq. (B.1) cancel for $\mathbf{u} = \mathbf{0}$ and the stability condition reduces to the case of pure diffusion as expected. In Eq. (B.1) the flux of component $C$ is given by

$$\mathbf{J} = -D\nabla C + \mathbf{u}C. \tag{B.2}$$

Eq. (B.1) shows the loss of unconditional stability for the advection–diffusion scheme, even for a single component, as the velocity field can be such that $E^{out} > E^{in}$ locally.

## References


[1] P. Bhatnagar, E. Gross, A. Krook, A model for collisional processes in gases I: small amplitude processes in charged and neutral one-component system, Physical Review 94 (1954) 511–525.
[2] B. Chopard, M. Droz, Cellular Automata and Modeling of Physical Systems, Monographs and Texts in Statistical Physics, Cambridge University Press, 1998. p. 353.
[3] B. Chopard, P. Luthi, A. Dupuis, Cellular automata and lattice Boltzmann techniques: an approach to model and simulate complex systems, Advances in Complex Systems 5 (2002) 103–246.
[4] B. Chopard, J.-L. Falcone, J. Latt, The lattice Boltzmann advection–diffusion equation revisited, European Physical Journal 171 (2009) 245–249.
[5] G. Drazer, J. Koplik, Tracer dispersion in two dimensional rough fractures, Physical Review 63 (2001) 11.
[6] D. D'Humières, Generalized lattice Boltzmann equations, AIAA Rarefied Gas Dynamics: Theory and Simulations. Progress in Astronautics and Aeronautics 59 (1992) 450–548.
[7] D. D'Humières, I. Ginzburg, M. Krafczyk, P. Lallemand, L.S. Luo, Multiple-relaxation-time lattice Boltzmann models in three dimensions, Philosophical Transactions of the Royal Society of London, Series A 360 (2002) 437–451.
[8] A.R. Felmy, J.H. Weare, Calculation of multicomponent ionic diffusion from zero to high concentration: I. The system Na-K-Mg-Cl-$SO_4$-$H_2O$ at 25 C, Geochemica et Cosmochimica Acta 55 (1991) 113–131.
[9] A.R. Felmy, J.H. Weare, Calculation of multicomponent ionic diffusion from zero to high concentration: II. Inclusion of associated ion species, Geochemica et Cosmochimica Acta 55 (1991) 133–144.
[10] U. Frisch, B. Hasslacher, Y. Pomeau, Lattice gas automata for the Navier–Stokes equations, Physical Review Letters 56 (1986) 1505–1508.
[11] I. Ginzburg, Equilibrium-type and link-type lattice Boltzmann models for generic advection and anisotropic-dispersion equation, Advances in Water Resources 28 (2005) 1171–1195.
[12] I. Ginzburg, Generic boundary conditions for the lattice Boltzmann models and their application to advection and anisotropic dispersion equations, Advances in Water Resources 28 (2005) 1196–1216.
[13] I. Ginzburg, D. D'Humières, Lattice Boltzmann and analytical modeling of flow processes in anisotropic and heterogenous stratified aquifers, Advances in Water Resources 30 (2007) 2202–2234.
[14] Z. Guo, B. Shi, C. Zheng, A coupled lattice BGK model for the Boussinesq equations, International Journal for Numerical Methods in Fluids 39 (5) (2002) 325–342.
[15] Z. Guo, T.S. Zhao, Lattice Boltzmann simulation of natural convection with temperature-dependent viscosity in a porous cavity, Progress in Computational Fluid Dynamics 5 (2005) 110–117.
[16] C.E. Harvie, J.H. Weare, The prediction of mineral solubilities in natural waters: the Na-K-Mg-Ca-Cl-$SO_4$-$H_2O$ system from zero to high concentration at 25 C, Geochemica et Cosmochimica Acta 44 (1980) 981–997.
[17] C.E. Harvie, N. Møller, J.H. Weare, The prediction of mineral solubilities in natural waters: the Na-K-Mg-Ca-H-Cl-$SO_4$-OH-$HCO_3$-$CO_3$-$CO_2$-$H_2O$ system to high ionic strengths at 25 C, Geochemica et Cosmochimica Acta 48 (1984) 723–751.

[18] F.J. Higuera, J. Jimenez, Boltzmann approach to lattice gas simulations, Europhysics Letters 9 (1989) 663–668.
[19] C. Huber, A. Parmigiani, B. Chopard, M. Manga, O. Bachmann, Lattice Boltzmann model for melting with natural convection, International Journal of Heat and Fluid Flow (2008), doi:10.1016/j.ijheatfluidflow.2008.05.002.
[20] S.E. Ingebritsen, W.E. Sanford, Groundwater in Geologic Processes, Cambridge University Press, 1998, 365 p.
[21] Q. Kang, P.C. Lichtner, D. Zhang, An improved lattice Boltzmann model for multicomponent reactive transport in porous media at the pore scale, Water Resources Research 43 (2007) W12S14.
[22] R. Kumar, S.S. Nivarthi, H. Ted Davis, D.M. Kroll, R.S. Maier, Application of the lattice-Boltzmann method to study flow and dispersion in channels with and without expansion and contraction geometry, International Journal for Numerical Methods in Fluids 31 (1999) 801–819.
[23] E. Kozeschnik, Multicomponent diffusion simulation based on finite elements, Metallurgical and Materials Transactions A: Physical Metallurgy and Materials Science 30 (1999) 2575–2582.
[24] A. Lerman, B.F. Jones, Transient and steady-state salt transport between sediments and brine in closed lakes, Limnology and Oceanography 18 (1973) 72–85.
[25] D.G. Miller, Application of irreversible thermodynamics to electrolyte solutions. I. Determination of ionic transport coefficients $l_{ij}$ for isothermal vector transport processes in binary electrolyte systems, Journal of Physical Chemistry 70 (8) (1966) 2639–2659.
[26] D.G. Miller, Application of irreversible thermodynamics to electrolyte solutions. II. Ionic coefficients $l_{ij}$ for isothermal vector transport processes in ternary systems, Journal of Physical Chemistry 71 (3) (1967) 616–632.
[27] D.G. Miller, Application of irreversible thermodynamics to electrolyte solutions. III. Equation for isothermal vector transport processes in $n$-component systems, Journal of Physical Chemistry 71 (11) (1967) 3588–3592.
[28] L. Onsager, R.M. Fuoss, Irreversible processes in electrolytes. Diffusion, conductance, and viscous flow in arbitrary mixtures of strong electrolytes, Journal of Physical Chemistry 36 (1932) 2689–2778.
[29] L. Onsager, The motion of ions: principles and concepts, Science 166 (1969) 1359–1364.
[30] Y.H. Qian, D. D'Humières, P. Lallemand, Lattice BGK models for the Navier–Stokes equation, Europhysics Letters 17 (1992) 479–484.
[31] F.L. Sayles, The composition and diagenesis of interstitial solutions – II. Fluxes and diagenesis at the water-sediment interface in the high latitude North and South Atlantic, Geochemica et Cosmochimica Acta 45 (1981) 1061–1086.
[32] B. Servan-Camas, F.T.-C. Tsai, Lattice Boltzmann method with two relaxation times for advection–diffusion equation: third order analysis and stability analysis, Advances in Water Resources 31 (2008) 1113–1126.
[33] X. Shan, Simulation of Rayleigh–Benard convection using a lattice Boltzmann method, Physical Review E 55 (5) (1997) 2780–2788.
[34] S. Succi, The Lattice Boltzmann Equation, for Fluid Dynamics and Beyond, Oxford University Press, 2001. 288 p..
[35] S. Suga, Numerical schemes obtained from lattice Boltzmann equations for advection–diffusion equations, International Journal of Modern Physics C 17 (11) (2006) 1563–1577.
[36] R.G.M. van der Sman, Diffusion on unstructured triangular grids using lattice Boltzmann, Future Generation Computer Systems 20 (2004) 965–971.
[37] R.G.M. van der Sman, Galilean invariant lattice Boltzmann scheme for natural convection on square and rectangular lattices, Physical Review E 74 (2006) 026705.
[38] D.A. Wolf-Gladrow, Lattice-Gas Cellular Automata and Lattice Boltzmann Models: An Introduction, Lecture Notes in Mathematics, Springer, 2000. p. 308.
[39] X. Zhang, J.W. Crawford, A.G. Bengough, I.M. Young, On boundary conditions in the lattice Boltzmann model for advection and anisotropic dispersion equation, Advances in Water Resources 25 (2002) 601–609.